THE ASTROPHYSICAL JOURNAL, 402:15–41, 1993 January 1

TIDALLY TRIGGERED GALAXY FORMATION. II. GALAXY NUMBER COUNTS

CEDRIC LACEY[1]
Physics Department, Oxford University, Astrophysics Building, Keble Road, Oxford OX1 3RH
BRUNO GUIDERDONI[2] AND BRIGITTE ROCCA-VOLMERANGE[3]
Institut d'Astrophysique, 98 bis, Boulevard Arago, F-75014 Paris, France
AND
JOSEPH SILK[4]
Astronomy Department, University of California, Berkeley, CA 94720
Received 1991 December 16; accepted 1992 June 25

ABSTRACT

We present a model for the evolution of the galaxy luminosity function, based on a scenario in which galaxies form by hierarchical clustering of a dynamically dominant dark matter component, and in which the rate of star formation is controlled by the frequency of tidal interactions with neighboring galaxies. We apply this to a cosmology with $\Omega = 1$, and in which the initial spectrum of density fluctuations is that predicted by the cold dark matter model. The properties of galaxy halos are calculated using the formalism for peaks in a Gaussian density field. The gas in galaxy halos is required to cool before it can form stars and is assumed to collapse dissipatively by a constant factor relative to the halo. Energy injection by supernovae is assumed to drive mass loss from low-mass galaxies. There is no merging of the luminous parts of galaxies. The luminosities and colors of stellar populations are calculated using a spectral evolution model, including the effects of internal extinction. We present results for the present luminosities, colors, mass-to-light ratios, surface brightnesses, and circular velocities of present-day galaxies, and for the numbers, colors and redshifts of the galaxies seen in the faint counts, and make a detailed comparison with the available observational data. For our standard model, we find good fits to the present luminosity function for bright galaxies and to the surface brightness-luminosity relation, and consistency with the Tully-Fisher relation for spirals. We find a reasonable fit to the galaxy number counts in the *B*-band over the whole range of magnitudes observed, with the faintest counts being dominated by mass-losing dwarf galaxies at redshifts $z \sim 0.2$–1. We find consistency with the color distributions at brighter magnitudes, when we include a significant component of extra extinction applied to massive OB stars only. We also obtain satisfactory fits to the redshift distributions of faint galaxies, except for an excess at $z \lesssim 0.1$ due to having a steep present luminosity function. Our models are deficient in red bright galaxies at the present day, a problem that could probably be solved by including a modest amount of merging. The faint-end slope predicted for the present-day luminosity function is at least as steep as that found in the Virgo and Fornax clusters and is steeper than that found in the field, in so far as that is known at faint magnitudes. In fact, our model implies that luminous galaxies have not formed in underdense regions because no tidal interactions have occurred to trigger star formation. Instead, there would be dark galaxies, with all their baryons in the form of cool gas. Possible observational counterparts of these gas-rich systems would include Lα clouds seen in absorption toward quasars; however, a full discussion of the implications of the present model for the observability of such systems in the field remains to be developed.

Subject headings: dark matter — galaxies: formation — galaxies: fundamental parameters — galaxies: interactions — galaxies: luminosity function, mass function — stars: formation

1. INTRODUCTION

Models for the formation of galaxies and large-scale structure have become increasingly sophisticated both in terms of their treatment of the growth of the small-amplitude seed fluctuations at early times and of the nonlinear evolution by gravitational clustering at late times, allowing detailed predictions to be made of the distribution and dynamics of the dominant mass component, if this is assumed to be some form of collisionless dark matter. On the other hand, most of our knowledge about the evolution of structure comes from studying that fraction of the matter which has become luminous by forming stars. In recent years, increasingly detailed observational data have been obtained, in the form of number counts, color distributions, and redshift distributions, which provide information about the evolution of luminous galaxies from early epochs up to the present. Theoretical modeling of the galaxy luminosity function is central to the interpretation of this data. Yet, up to now, there has been relatively little work on relating the galaxy luminosity function to models for structure formation.

In most present models for structure formation, most of the mass in the universe is assumed to be in some collisionless, dark form, typically some species of weakly interacting elementary particle, with only a small admixture of baryons, initially in gaseous form. The baryons thus have almost negligible influence on the dynamics of the dark matter, whose evolution can therefore be calculated using only gravitational physics. Thus, using either *N*-body simulations or analytical approximations, one can predict the spatial distribution, masses, sizes, and for-

[1] Email: 19813::cgl (SPAN); cgl@dionysos.thphys.ox.ac.uk (Internet).
[2] Email: 17649::guider (SPAN); guider@friap51 (Bitnet).
[3] Email: 17649::brigit (SPAN); rocca@friap51 (Bitnet).
[4] Email: 42215::silk (SPAN); silk@bkyast.berkeley.edu (Internet).

mation times of galaxy halos. Going beyond this to predict the distribution and properties of the luminous matter involves much more complicated and less well understood physics, namely: (1) the dissipative collapse of baryons within dark halos, including shock heating and radiative cooling of the gas, and, at a later stage, energy injection into the gas by young stars; (2) the formation of stars from the gas once it has cooled and formed dense clumps. While the basic physics of dissipation are understood (but the details are complicated because of the highly nonlinear processes involved), there is currently no predictive theory of star formation at all. These difficulties have until recently deterred most galaxy formation theorists from going beyond very simple schemes for relating mass to light, for instance assuming a constant luminosity-to-mass ratio for all galaxy halos. Such models are completely inadequate for interpreting the observational data on number counts, and color and redshift distributions, which are now becoming available.

In contrast, many other astronomers have followed a different, more phenomenological approach to investigating luminosity function evolution, independent of theoretical models for galaxy formation (which were, in any case, not so well developed when this type of work began), instead taking the observed properties of the present-day galaxy population as a starting point, and trying to work backward from there.

This approach is based on models of the photometric or spectroscopic evolution of galaxies, such as those developed by Tinsley (1980), Rocca-Volmerange, Lequeux, & Maucherat-Joubert (1981), Bruzual (1981, 1983 hereafter B83), Arimoto & Yoshii (1986, 1987), and Guiderdoni & Rocca-Volmerange (1987, hereafter GRV87). The physical foundation of these works is the theory of stellar evolution, but in order to relate the past evolution to present properties, this must be supplemented by various assumptions of a more phenomenological nature: (1) galaxies are divided into types based on their present colors, and all galaxies of the same type are assumed to have the same dependence of the star formation rate on time (independent of mass), which is usually assumed to be exponential in time, or proportional to the gas mass, and is parameterized by a star formation time scale. (2) Galaxies of a given type are assumed to all begin forming stars at a single redshift. (3) Galaxies of a given type are assumed to have a mass function of a simple analytical form, typically a Schechter function; almost all models have in addition assumed no evolution in the mass function after the epoch of formation. This last assumption has, however, been relaxed in recent papers by Rocca-Volmerange & Guiderdoni (1990) and Guiderdoni & Rocca-Volmerange (1991), who investigated a phenomenological model of mass function evolution. Some versions of these models also include the evolution of the gas content, a consistent calculation of internal extinction, the influence of metallicity, and nebular emission. By themselves, these models allow one to study the sensitivity of the luminosity and colors of a galaxy's stellar population to a number of crucial parameters, such as the characteristic time scale for star formation, the age, the initial mass function, and the metallicity. As an example, it is easy to reproduce the variation of spectrophotometric properties along the present Hubble sequence by varying only the time scale for star formation (e.g., Rocca-Volmerange & Guiderdoni 1988). Such preliminary work is of great interest for determining the most important parameters controlling the spectrophotometric properties of galaxies in the various wavelength ranges. In addition to that exploration, the models allow one to test some simple, phenomenological ideas about galaxy evolution, by extrapolating the current luminosity and colors of galaxies back into the past.

This phenomenological approach has recently had considerable success in constraining galaxy evolution and cosmological parameters using the results of deep galaxy surveys (Bruzual & Kron 1980; Yoshii & Takahara 1988; Guiderdoni & Rocca-Volmerange 1990a; Metcalfe et al. 1991; Yoshii & Peterson 1991). The deep surveys probe the field galaxy population and are also sensitive to space curvature through the dependence of the volume element on redshift. They are sensitive to the intrinsic evolution of "average" galaxies, which may be more easily modeled than that of extreme objects such as the hosts of high-redshift radio-galaxies. The main conclusion of these studies, as emphasized by Guiderdoni & Rocca-Volmerange (1989, 1990), and Koo (1990) is that, if the galaxy mass function has a flat low-mass slope, $dn/dM \propto M^{-1}$, as suggested from extrapolation of the bright end of the observed present luminosity function, and if the mass function does not evolve with time, then the data cannot be fitted within an $\Omega_0 = 1$ cosmology. On the contrary, they suggest a low value of $\Omega_0 \sim 0.1$. This conclusion, given the assumptions (including points 1 and 2 above), is very robust and does not depend on the IMF, redshift of first star formation, or star formation history, provided these are independent of mass. This result follows most strongly from counts in the B-band, but is supported by modeling of the counts in the UV and other visible bands. (It does not seem to be required by the K-band counts, however.) Of course, a major weakness of the phenomenological approach is that it assumes that all galaxies started forming stars at a single redshift z_*, "the redshift of galaxy formation." This assumption cannot be correct, but going beyond it to allow a distribution of z_* requires introducing many more parameters, which are hard to constrain. The model we investigate in this paper in fact predicts a distribution of z_*, but we shall see in § 4.1 that this apparently does not alter the conclusion of the phenomenological approach: it is not possible to fit the faint counts within an $\Omega = 1$ universe while retaining a mass function which is nearly flat at low masses. (Needless to say, the details of the luminosity and color evolution are strongly modified by this new model.)

On the contrary, the deep redshift survey by Cowie, Songaila, & Hu (1991) suggests that there are a larger number of dwarf galaxies at $z \sim 0.3$ than are known nearby. Either we are seeing in the B-band counts an additional population of dwarf galaxies which are yet to be discovered in local surveys (Cole, Treyer, & Silk 1992) or there is strong number and mass evolution, so that these dwarfs have by now turned into something else (Koo 1990; Rocca-Volmerange & Guiderdoni 1990; Guiderdoni & Rocca-Volmerange 1991). This putative dwarf population appears to have less effect on the K-band counts, which can be fitted with models involving only normal bright galaxies undergoing conventional luminosity evolution. In order to reconcile these results with having $\Omega = 1$, it seems necessary for the faint end slope of the luminosity function to steepen (from $\alpha \approx -1$ to $\alpha \approx -1.5$), or for the number density of galaxies to evolve [as $(1 + z)^{1.5}$] due to merging. In the current paper, the faint counts are reproduced by means of a large population of dwarfs which is predicted on the basis of a physical model, but this results in problems at the present epoch. We shall come back to the possible interpretation of the faint counts in terms of merging and number evolution in the discussion below.

It is obviously desirable to bring the ab initio and phenomenological approaches to galaxy luminosity function evolution closer together. By doing so, one should learn about both galaxy formation and star formation and about other galaxy evolution processes which affect the luminosity function, such as mass loss from galaxies via winds, and merging of galaxies. In addition, one can hope to shed some light on the problem of "biased galaxy formation": dynamical estimates of the mass associated with galaxy halos and with groups and clusters of galaxies suggest that Ω_0, the present ratio of the mean density of the universe to the critical density, has a value $\Omega_0 \approx 0.2$. On the other hand, theoretical arguments, including the inflationary universe paradigm, and observational constraints on specific galaxy formation models suggest that $\Omega_0 = 1$. To reconcile these two values, it seems that galaxy formation must be biased toward high-density regions, leading to luminous galaxies being more clustered than the dark matter. At present, there are no workable physical models for how this biasing should occur, only ad hoc schemes (e.g., identifying luminous galaxies with the highest peaks of the initial density field), but presumably biasing must be related to the processes of dissipation, star formation, and galaxy mass loss.

The largest uncertainty in any model which tries to relate the luminosity function to ideas about structure formation concerns the assumptions about star formation. It is not even clear whether the rate of conversion of gas into stars is controlled mainly by dynamical processes causing compression of the gas (e.g., spiral arms, collisions, and interactions of galaxies), or by some sort of balance between energy injection by young stars and radiative cooling (either locally in the interstellar medium or on a galaxy-wide scale, involving galactic fountains or winds). Therefore, it seems necessary to investigate various more-or-less phenomenological star formation models, incorporating one or more of these ideas, and see what observational consequences they lead to when combined with a scenario for galaxy formation. In this paper, we investigate a model, proposed by Lacey & Silk (1991, hereafter Paper I), based on the idea that the time scale for star formation is controlled by the frequency of dynamical interactions between galaxies. A different model based on the energy-balance approach has recently been investigated by White & Frenk (1991, hereafter WF). WF made approximate estimates of galaxy luminosities, but ours is the first ab initio model to attempt to predict galaxy colors, which in principle provide important constraints on galaxies' star formation histories.

The basic motivation and principles of this model were set out in Paper I, where more details are given. The primary motivation is the observation that star formation rates in spiral galaxies are enhanced over their average values in galaxies that are interacting, as follows from the work on *UBV* colors beginning with Larson & Tinsley (1978), and on ratios of Hα and far-infrared to optical luminosities (e.g., Lonsdale et al. 1984; Kennicutt et al. 1987). A second, less direct, motivation is the morphology-density relation for galaxies (e.g., Dressler 1980; Postman & Geller 1984), showing that the proportion of elliptical and S0 galaxies (with old stellar populations) relative to spirals (with younger populations) is larger in denser environments, and thus that the typical time scale for star formation is also smaller where the number density of galaxies is larger. Qualitatively, it is not so surprising that galaxy interactions enhance the star formation rate, since the time-dependent tidal gravitational field during an encounter will cause compression and shocking of the gas, especially in a disk galaxy (see the review by Noguchi 1990). However, the observations (e.g., Kennicutt et al. 1987) indicate that the fraction of all current star formation that is occurring in galaxies that are strongly interacting is only $\sim 10\%$. Our model makes the much more sweeping assumption that essentially *all* star formation is associated with galaxy interactions in some way. To reconcile this with the observations, we have to argue that quite weak encounters (with small or distant galaxies) can be effective, and/or that the influence of an encounter on the star formation rate lasts several times longer than the encounter itself. For instance, spiral structure in stellar disks might require intermittent external forcing to keep going over a Hubble time, with the spiral pattern induced by a single tidal encounter lasting for several rotation periods (Toomre 1981; Noguchi 1990).

Paper I described the basic formalism for the model, which we also adopt in this paper, but with a few extensions. The starting point is the initial, linear, density fluctuation field. Peaks in this field are identified with incipient galaxy halos, whose collapse is described by a spherical model. The gas in each halo is assumed to condense to form a baryonic core if it satisfies a cooling condition. Star formation is assumed to begin in each core once the surrounding group collapses and galaxy interactions begin. However, there is assumed to be no merging of the baryonic cores, i.e., of the luminous components of galaxies, even if the halos merge. The star formation time scale is assumed to be proportional to the galaxy encounter time. The distributions of galaxy masses, formation times, encounter times, etc., are then calculated using the formalism for peaks in a Gaussian density field. We have assumed in our detailed modeling that the power spectrum of the initial fluctuations is that predicted by the cold dark matter (CDM) model, with cosmological parameters $\Omega = 1$ and $H_0 = 50$ km s^{-1} Mpc^{-1}, since this seems to provide a good description of galaxy clustering on scales $\sim$(0.1–10) Mpc, but our star formation model could in principle be applied for any fluctuation spectrum which resulted in hierarchical formation of structure. Star formation feedback is included in the model, in that galaxies having sufficiently low escape velocities are assumed to lose most of their gas through a supernova-driven wind. Given the analytically predicted distribution of galaxy masses and star formation parameters, we then compute the spectrophotometric evolution of each galaxy using a stellar population synthesis model.

In Paper I, we mainly considered the predictions of our model for the present luminosity and color distributions of galaxies and only briefly considered the problem of galaxy number counts. However, the predictions of the model for the form of the luminosity function at high redshifts are the most exciting, and so in this paper we will make a detailed comparison of the model results with the observational data constraining this evolution, namely, the galaxy number counts to faint magnitudes, and the corresponding color and redshift distributions.

We have made a number of improvements in the model compared with Paper I. (1) We use a more up-to-date spectrophotometric evolution model, that of Guiderdoni & Rocca-Volmerange (1987, recently upgraded as described in Rocca-Volmerange 1992), instead of that of Bruzual (1983). The former model is based on more recent stellar data, including more stages of stellar evolution, and includes the effects of dust extinction and emission from ionized gas. It also overcomes a number of computational limitations in Bruzual's code. (2) We extend our model to include a consistent treat-

ment of the dwarf galaxies, which lose mass via winds. In our model, these dwarf galaxies make the dominant contribution to the number counts at the faintest magnitudes. (3) We explicitly model the radii of the luminous components of galaxies, allowing a comparison with observational data on the surface brightnesses of galaxies, and a consistent calculation of isophotal corrections to the magnitudes of galaxies seen in the counts. We also calculate the relation between the halo circular velocity and luminosity, and compare with the observations.

The plan of this paper is as follows: § 2 describes how the model is constructed. Section 3 gives the predictions for the present properties of galaxies and compares to the observations. Section 4 compares the model predictions with observations of galaxy number counts. Section 5 presents some of the predictions of the model which are of interest for future observations. Section 6 discusses our main results and considers the problems outstanding. Preliminary results of some of this work were reported in Guiderdoni & Rocca-Volmerange (1990b) and Lacey (1991).

2. CONSTRUCTION OF THE MODEL

In our model, we attempt to derive the luminosity function of the final galaxy population directly from a dynamical model for structure formation, together with a model for star formation. Our model for structure formation is fairly standard: we assume that the universe has the critical density ($\Omega = 1$), with baryonic matter making up a few percent of this, and the remainder being some form of collisionless dark matter. Structure is assumed to form by the growth due to gravity of initially small density fluctuations. These initial density fluctuations are assumed to obey Gaussian statistics and to have a power spectrum such that the typical amplitude decreases with scale, so that small objects form first, and larger objects form later, i.e., structure grows hierarchically. For the sake of definiteness, we have taken the initial fluctuation spectrum to be that predicted in the standard cold dark matter (CDM) model, in which the dark matter is in the form of some weakly interacting elementary particle with initially negligible velocity dispersion (e.g., Blumenthal et al. 1984). This seems to provide a reasonable fit to the properties of galaxy halos and galaxy clustering up to scales ~ 10 Mpc (e.g., Davis et al. 1985; Frenk et al. 1988). Some observations indicate that the CDM spectrum may contain too little power on large scales, but this would not affect the predictions of our model, which depends only on the form of the power spectrum on galaxy scales. Galaxy halos form by the dissipationless evolution of the dark matter, and baryonic cores then form by the cooling and gravitational condensation of the gas within these halos (White & Rees 1978). Our model for the rate at which star formation occurs within these baryonic cores is more speculative: we assume that the time scale for star formation in each galaxy is controlled by the density of the local environment through the frequency of interactions with neighboring galaxies. The final efficiency of the conversion of gas into stars is modulated by the effects of feedback: galaxies having low escape velocities (shallow potential wells) are assumed to lose some fraction of their gas through a galactic wind driven by energy input from supernovae (Dekel & Silk 1986). The luminosity evolution of each galaxy is then computed using a spectral evolution code based on theoretical stellar evolutionary tracks.

Most parts of the formulation of our model have been discussed in detail in Paper I, so we will just review them here. We have extended the model in two ways: (1) we consider explicitly the radii of the baryonic cores formed by condensation within dark halos, allowing us to calculate the surface brightness of the luminous galaxies formed. (2) We model the amount of mass loss due to feedback, to allow a treatment of the luminosity function of dwarf galaxies. (In Paper I, we only considered in detail the luminosity function of the bright galaxies, for which mass loss was assumed to be negligible.) These latter two aspects will be described here in more detail. We also use an improved model for spectrophotometric evolution, that of Guiderdoni & Rocca-Volmerange, as we describe below.

2.1. *Halo Formation*

We model the distribution of halo masses and formation redshifts analytically. Our starting point is the density fluctuation field, $\delta \equiv \delta\rho/\bar{\rho} \equiv \rho/\bar{\rho} - 1$ ($\bar{\rho}$ being the cosmological mean density) in the linear regime, $\delta \ll 1$. In linear perturbation theory, δ when considered as a function of comoving coordinates $\boldsymbol{x}$ evolves as $\delta(x, t) = [D(t)/D(t_i)]\delta(\boldsymbol{x}, t_i)$, where for $\Omega = 1$ the linear growth factor is $D(t) \propto t^{2/3} \propto 1/(1 + z)$, z being the redshift, and t_i some arbitrary reference time. It is convenient in what follows to define comoving coordinates to coincide with physical coordinates at the present epoch, $t = t_0 = \frac{2}{3}H_0^{-1}$, and to work in terms of the fluctuation amplitude extrapolated to $t = t_0$ according to linear theory; we employ the notation $\delta(\boldsymbol{x}) \equiv [D(t_0)/D(t_i)]\delta(\boldsymbol{x}, t_i)$. Each galaxy halo is assumed to originate from a peak in the initial density fluctuation field, having overdensity δ_g and comoving radius R_g. The comoving radius is related to the mass by

$$M_g = \frac{4\pi}{3}\bar{\rho}_0 R_g^3 , \tag{1}$$

where $\bar{\rho}_0 = 3H_0^2/8\pi G$ is the present mean density. The nonlinear evolution, collapse, and virialization of each dark halo are then calculated using a spherical "top-hat" collapse model. According to this, collapse of the halo occurs at a time

$$t_{f,g} = (\pi/H_0)(3/5\delta_g)^{3/2} , \tag{2}$$

when the linearly extrapolated overdensity has a value $\delta_{cr} = 1.69$. If the virialized halo is modeled as a uniform sphere, it has a physical radius

$$r_g = (3/10\delta_g)R_g , \tag{3}$$

and a three-dimensional velocity dispersion

$$v_g = (3GM_g/5r_g)^{1/2} = H_0 R_g \delta_g^{1/2} . \tag{4}$$

If we instead model the halo as a truncated singular isothermal sphere with the same mass and binding energy, then v_g is the circular velocity for the halo.

To calculate the comoving number density n_{pk} of peaks as a function of overdensity δ_g and mass M_g, we use results for the statistics of peaks in a Gaussian random field derived by Bardeen et al. (1986, hereafter BBKS). In fact, the expression we assume for the star formation time scale in a galaxy depends also on the mass and density of the surrounding galaxy group, which depend in turn on the overdensity δ_{gr} and comoving radius R_{gr} of the group in the linear regime, according to the same spherical collapse model as assumed for the galaxy halo. We assume that the group mass is always a fixed multiple of the mass of the galaxy halo, i.e., $M_{gr}/M_g =$ constant. The differential number density of peaks relative to the three independent variables (M_g, δ_g, δ_{gr}) can then be written

as

$$\frac{d^3 n_{\rm pk}}{dM_g\, d\delta_g\, d\delta_{\rm gr}} = \frac{dn_{\rm pk}}{dM_g} P\left(\delta_g, \delta_{\rm gr}; M_g, \frac{M_{\rm gr}}{M_g}\right). \quad (5)$$

where $P(\delta_g, \delta_{\rm gr})$ is normalized so that $\iint P(\delta_g, \delta_{\rm gr}) d\delta_g\, d\delta_{\rm gr} = 1$. As discussed in Paper I, we take $dn_{\rm pk}/dM_g$ to be the derivative with respect to mass of the total number density of peaks in the field when smoothed on scale M_g, and $P(\delta_g, \delta_{\rm gr})$ to be the probability density of one of these peaks having overdensity δ_g and being in a background (smoothed on scale $M_{\rm gr}$) of overdensity $\delta_{\rm gr}$, using the expressions given by BBKS. The use of equation (5) is then only an approximation. (To convert eqs. [2.4] and [2.6] of Paper I into the form used here note that the Gaussian filter radius R_f used there is related to the "top-hat" radius R used here by $R_f = (4\pi/3)^{1/3}(2\pi)^{-1/2} R$, while the normalized overdensity ν is related to the actual overdensity δ by $\nu = \delta/\sigma(M)$, $\sigma(M)$ being the rms fluctuation on mass scale M.) We adopt $M_{\rm gr}/M_g = 8$, corresponding to $R_{\rm gr}/R_g = 2$.

The expression for the distribution of peak properties depends on the assumed power spectrum of the fluctuations. We have used the fit to the CDM power spectrum given by BBKS, normalized in terms of σ_8, the rms density fluctuation in a sphere of radius $8h^{-1}$ Mpc, or equivalently in terms of the "bias parameter" $b \equiv 1/\sigma_8$. The value of b is somewhat uncertain. Davis et al. (1985) favored a value $b = 2.5$, mainly based on comparing their N-body simulations to the galaxy-galaxy velocity dispersion on a scale $r \sim 1h^{-1}$ Mpc. On the other hand, studies of galaxy flustering (e.g., Maddox et al. 1990a, b) and streaming velocities (e.g., Dekel 1991) on larger scales ($r \sim 10$–$50h^{-1}$ Mpc) have favored smaller values, around $b \approx 1.5$. Recently, Carlberg (1991) has even suggested that the galaxy-galaxy velocity dispersion on small scales can be reconciled with the large-scale power for a value of b as low as 1.0 through the mechanism of "velocity bias." We will therefore adopt $\sigma_8 = 0.5$ ($b = 2$) as our standard value, as in Paper I, but investigate the effect of varying σ_8 in the range 0.4 to 0.7 ($1.4 < b < 2.5$).

We assume throughout that the present Hubble constant is $H_0 \equiv 100h$ km s^{-1} Mpc^{-1} = 50 km s^{-1} Mpc^{-1}. The fraction of mass in the form of baryons, $f_b \equiv \Omega_b/\Omega$, can be constrained by comparing abundances of light elements with the predictions of primordial nucleosynthesis, which gives $0.03 \lesssim f_b \lesssim 0.10$ according to Kawano, Schramm, & Steigman (1988), and $0.04 \lesssim f_b \lesssim 0.06$ according to Walker et al. (1991). In this paper, we adopt a standard value $f_b = 0.06$ (compared to $f_b = 0.07$ in Paper I), but investigate the effects of varying f_b over the range 0.04–0.09.

2.2. *Formation of Baryonic Cores*

Within each dark halo, the baryons in the form of gas are assumed to be shock heated to the virial temperature of the halo at the time the halo collapses. If the gas has sufficient time to cool by radiation, then it settles within the halo to form a dense baryonic core at the center. We compute the cooling time $t_{\rm cool}$ treating the halo as having a uniform density and using the cooling function for gas of primordial composition given by Fall & Rees (1985). The time available for cooling is assumed to be the difference in collapse times of the galaxy halo and of the surrounding group. Thus, our condition for forming a baryonic core in a given galaxy halo is simply

$$t_{\rm cool} < t_{f,\rm gr} - t_{f,g}\,, \quad (6)$$

where the collapse times are calculated from the linear overdensities using equation (2), and galaxy and group scales are related as described above. If this condition is not satisfied, the gas is assumed to be reheated and dispersed into the group halo when the group itself collapses.

Once a baryonic core has formed, it is assumed to survive all subsequent merging of halos. Thus our model does not include any merging of luminous galaxies. At present, numerical simulations do not reliably predict the amount of merging of the baryonic components of galaxies, and the main justification for this no-merger assumption comes from observations of galaxy morphology, which indicate that most luminous galaxies cannot have suffered major mergers since they formed most of their gas into stars.

Our model neglects the fact that the total gas supply available for forming baryonic cores by cooling decreases with time, due to the formation of baryonic cores in previous generations of dark halos. However, this is not too serious, as even by the present day, most of the baryons in our model are still in diffuse form. The cooling function we use cuts off at $T \lesssim 10^4$ K, and this sets a natural limit to the fraction of baryons which can cool. If the gas is heated by an ionizing background, this could suppress even further the formation of baryonic cores in low-mass halos, as discussed by Efstathiou (1992).

We assume that the (three-dimensional) half-mass radius of the baryonic core which forms by dissipative collapse is a constant fraction $f_{\rm diss}$ of the radius r_g of its parent halo. This can be approximately justified for disk galaxies by noting that for gas which collapses down to a centrifugally supported state within an isothermal dark halo while conserving its specific angular momentum, the collapse factor is $f_{\rm diss} \sim \lambda_{\rm H}$ (Fall 1983), where $\lambda_{\rm H}$ is the dimensionless spin parameter of the gas, assumed to be initially the same as that of the halo. N-body simulations show that halos typically have $\lambda_{\rm H} \approx 0.05 \pm 0.03$ (mean and standard deviation) as a result of tidal torquing, with only a weak dependence on the mass or the form of the initial fluctuation spectrum (Barnes & Efstathiou 1987; Zurek, Quinn, & Salmon 1988; Efstathiou et al. 1988). Thus one expects $f_{\rm diss} \sim 0.1$ for disk galaxies. According to this argument, one also expects a spread in collapse factors (by a factor of 2 either way). For spheroidal galaxies, the above argument cannot be applied directly, as the stellar population is not rotationally supported. For simplicity, however, we shall assume that a single constant collapse factor applies, regardless of geometry, to both protodisks and protospheroids. In the models, the value of $f_{\rm diss}$ is adjusted to give a reasonable fit to the radii of luminous galaxies. (The value we obtain by fitting is $f_{\rm diss} = 0.05$, in reasonable agreement with our theoretical expectations for disk formation.)

2.3. *Star Formation Rate*

A crucial assumption of our model is that the rate of conversion of gas into stars in the baryonic cores is controlled by the frequency of interactions with other galaxies in the group. Thus, star formation begins in a galaxy only after the surrounding group has collapsed. This gives for the redshift z_* at which star formation turns on

$$1 + z_* = \delta_{\rm gr}/\delta_{\rm cr}\,. \quad (7)$$

Once star formation has begun, it is assumed to proceed on a time scale τ_*, such that the rate of formation of new stars Ψ is

$$\Psi(t) = M_{{\rm gas},g}(t)/\tau_*\,, \quad (8)$$

where $M_{\rm gas,g}$ is the instantaneous gas mass. In Paper I, we suggested the following expression for the star formation time scale, based on the idea that this should be proportional to the mean time between galaxy encounters in the group, with the encounter cross section being proportional to the geometrical cross section of the halo:

$$\tau_* = \frac{1}{A_*}\frac{t_{d,\rm gr}}{N_{\rm gr}}\left(\frac{r_{\rm gr}}{r_g}\right)^2 = \left(\frac{\pi}{2}\right)\left(\frac{3}{5}\right)^{3/2}\frac{1}{H_0 A_*}\left(\frac{M_g}{M_{\rm gr}}\right)^{1/3}\left(\frac{\delta_g}{\delta_{\rm gr}}\right)^2\frac{1}{\delta_{\rm gr}^{3/2}} \quad (9)$$

where $N_{\rm gr} = M_{\rm gr}/M_g$ is the nominal number of galaxies in the group, and $t_{d,\rm gr} = \frac{1}{2}t_{f,\rm gr}$ is the group dynamical time. In this expression, the parameter A_* is adjusted to try to fit the present-day luminosity and color distributions of galaxies. We emphasize that mergers of the luminous parts of galaxies are specifically excluded in our model. Also, in calculating the star formation time scale, evolution in the group environment after star formation turns on, due to collapse on still larger scales, is ignored. The predictions of our model turn out to be much more sensitive to the distribution of turn-on redshifts z_* than to the precise values taken for τ_*.

An important consequence of our model for star formation is a form of biasing in the distribution of luminous matter relative to dark matter. This has two causes: (1) not all halos form baryonic cores (the cooling time of the gas may be too long); (2) not all baryonic cores form stars by the present (the group containing the galaxy may not yet have collapsed). As a consequence, the mass-to-light ratio of luminous galaxies (including the mass in their own dark halos) is less than that of the universe as a whole, which is necessary if the mass-to-light ratios measured for clusters and groups of galaxies are to be reconciled with having $\Omega = 1$ (Blumenthal et al. 1984; Davis et al. 1985). The amount of biasing in our model is affected by the value assumed for $R_{\rm gr}/R_g = (M_{\rm gr}/M_g)^{1/3}$. For our choice $R_{\rm gr}/R_g = 2$, the number density of luminous galaxies per unit mass is suppressed relative to the total number density of peaks by a factor of 4 at $M_b \sim 10^{11}\,M_\odot$ (see Paper I). In terms of the "peak threshold" model of BBKS, this is roughly equivalent to identifying galaxies with peaks above a threshold overdensity $\delta = \nu\sigma$, with $\nu \approx 2$, although our selection procedure differs in detail from this simple prescription (which anyway has no definite physical basis). Note that in our model, the effective ν-threshold depends on mass, and declines toward zero at low masses.

2.4. *Star Formation Feedback and Galaxy Mass Loss*

There are feedback effects associated with star formation because massive young stars inject substantial amounts of energy into the interstellar medium in the form of photoionizing radiation, stellar winds, and supernova explosions. If the escape velocity is small enough, the heating of the gas, especially by supernovae, may be enough to drive a wind removing gas from the galaxy, as proposed by Larson (1974) and by Dekel & Silk (1986). For a baryonic core within an isothermal dark halo, the ratio of escape velocity to virial (or circular) velocity is $v_{\rm esc}/v_g \approx 3$ for $f_{\rm diss} \sim 0.1$. In Paper I, we assumed that there was strong mass loss from galaxies having $v_g < v_{\rm crit} = 100$ km s^{-1}, and no mass loss from galaxies with $v_g > v_{\rm crit}$, and only considered the contribution to the luminosity function from the latter. In this paper, we wish to model consistently the contribution to the luminosity function and the galaxy counts from the dwarf galaxies with $v_g < v_{\rm crit}$, and so we must make some assumption about how much mass these galaxies lose. The details of supernova heating of the interstellar medium and of the mechanics of galactic winds are rather uncertain, so we have chosen to model this mass loss phenomenologically, as follows: a galaxy is assumed to form stars at the rate given by equations (8) and (9) above, until it has converted a fraction f_* of its baryons into stars, and then to lose its remaining gas and stop forming stars. Gas shed by dying stars after the wind phase is assumed simply to accumulate in the galaxy, so the final baryonic mass $M_{\rm bf} = f_* M_b$ includes both stars and a small amount of gas. We assume that f_* depends on the halo velocity dispersion as

$$f_* = f_{*\rm crit}(v_g/v_{\rm crit})^\gamma \quad (v_g < v_{\rm crit}) \qquad = 1 \quad (v_g > v_{\rm crit}) \quad (10)$$

with $f_{*\,\rm crit} \le 1$. This form for the mass loss is motivated by the paper of Dekel & Silk, who argue that radiative energy losses prevent catastrophic mass loss from galaxies with velocity dispersions exceeding $v_g \gtrsim 100$ km s^{-1}, the latter value being only weakly dependent on the various parameters in the problem. We therefore adopt $v_{\rm crit} = 100$ km s^{-1} in all our models. We also adopt $\gamma = 2$, based on a simple energy balance argument: if radiative losses are neglected, then the amount of mass lost, $M_{\rm ej}$, is given by equating the total supernova energy input with the energy required to eject the remaining gas from the galaxy:

$$\tfrac{1}{2}M_{\rm ej}\,v_{\rm esc}^2 = \eta_{\rm SN}\,E_{\rm SN}\,M_*\,, \quad (11)$$

where $M_* = M_b - M_{\rm ej}$ is the mass formed into stars, $\eta_{\rm SN}$ is the number of supernovae per unit mass of stars formed, and $E_{\rm SN}$ is the energy injected by each supernova. When $f_* = M_*/M_b \ll 1$, this implies $f_* \propto v_g^2$. Adopting the values $\eta_{\rm SN} \approx 4 \times 10^{-3}\,M_\odot^{-1}$ (based on our standard IMF with a minimum mass of 8 $M_\odot$ for Type II supernovae), $E_{\rm SN} \approx 10^{51}$ ergs and $v_{\rm esc}/v_g \approx 3$, and extrapolating the $f_* \propto v_g^2$ dependence to $v_g = v_{\rm crit}$, gives $f_{*\rm crit} \approx (v_{\rm crit}^2/2\eta_{\rm SN}E_{\rm SN})(v_{\rm esc}/v_g)^2 \approx 0.2$. If radiative losses reduce the efficiency of supernova energy injection even for $v_g \ll v_{\rm crit}$, then the value of $f_{*\rm crit}$ is increased. To allow for the uncertainties in the amount of mass loss, we have calculated models for two cases: "strong mass loss," with $\gamma = 2$ and $f_{*\rm crit} = 0.1$, and "moderate mass loss," with $\gamma = 2$ and $f_{*\rm crit} = 1$. For the latter case, the mass loss varies continuously through $v_g = v_{\rm crit}$.

When a galaxy loses its gas through a wind, the remnant stellar system expands in response to the reduced self-gravity. We can roughly estimate the amount of this expansion as follows: if the time scale for mass loss exceeds the orbital time of the stars, then they respond adiabatically, so that the radii of the orbits before and after mass loss are related approximately by $r_i M_i(r_i) = r_f M_f(r_f)$, where $M(r)$ is the total mass (baryons + dark matter) within radius r, and the subscripts i and f refer to the initial and final states, respectively. We apply this equation at the half-mass radius r_* of the stars, and assume that the halo can be treated as a singular isothermal sphere with mass profile $M_{\rm H}(r) = v_g^2\,r/G$, which responds rigidly to the mass loss. Thus, the half-mass radii r_{*i} and r_{*f} before and after mass loss obey

$$r_{*i}(\tfrac{1}{2}M_b + v_g^2\,r_{*i}/G) = r_{*f}(\tfrac{1}{2}f_*\,M_b + v_g^2\,r_{*f}/G) \quad (12)$$

where $r_{*i} = f_{\rm diss}\,r_g$. This equation is easily solved for r_{*f}/r_{*i}.

2.5. *Spectrophotometric Evolution*

In our model, we take the independent parameters for each galaxy to be its baryonic mass M_b, the redshift z_* at which it turns on star formation, and the time scale τ_* for star formation. These parameters can be related to the parameters $(M_g, \delta_g, \delta_{gr})$ of the peaks description, and thus the comoving number density of peaks as a function of (M_b, z_*, τ_*) can be derived using equation (5). The other parameters f_*, r_*, etc., are then given in terms of the primary variables (M_b, z_*, τ_*) through their dependence on $(M_g, \delta_g, \delta_{gr})$.

Given (M_b, z_*, τ_*), we calculate the spectrophotometric evolution of that galaxy using the model of GRV87. The star formation rate is calculated as a function of galactic age, including the effects of stellar mass loss on the gas content. Theoretical stellar evolution tracks are used to compute the distribution of stars in the H-R diagram, and a spectrum assigned to each group of stars according to its spectral type and luminosity class. The sum of these spectra then gives the synthetic spectrum of the whole stellar population as a function of time (or redshift). Finally, convolution of these evolving spectra (appropriately redshifted) with the response functions of the standard filters (B, V, R, etc.) gives luminosities, colors, apparent magnitudes, etc., including the effects of K-corrections and evolutionary corrections.

In Paper I, we used the spectral evolution model of Bruzual (1981; B83) to compute galaxy luminosities. The spectral evolution model of Guiderdoni & Rocca-Volmerange used here represents an advance over that of B83 in several respects: (1) it includes later stages of stellar evolution, (2) it is based on more recent stellar evolution calculations, and (3) it includes a treatment of internal extinction by dust, and of emission by ionized gas in the galaxy. We now detail some of these aspects.

2.5.1. *Stellar Inputs*

The stellar evolution tracks are a crucial input for spectrophotometric evolution models. All ab initio models of galaxy formation up to now, including the most recent ones (Paper I and WF) have used the old B83 model based on the Yale group's stellar tracks. These tracks were also used in the phenomenological fits to the Hubble sequence (B83; Rocca-Volmerange et al. 1981; Arimoto & Yoshii 1986; GRV87; Rocca-Volmerange 1989), and to the faint galaxy counts (Bruzual & Kron 1980; Yoshii & Takahara 1988; Guiderdoni & Rocca-Volmerange 1990a; Metcalfe et al. 1991). Moreover B83 used a semi-empirical giant branch with a weight stronger than the theoretical giant branches used in GRV87 and in Yoshii & Takahara. New stellar tracks by Maeder & Meynet (1988) appeared recently and are used in Rocca-Volmerange & Guiderdoni (1990), and Guiderdoni & Rocca-Volmerange (1991). These new tracks are now also included in the new model by Charlot & Bruzual (1991) which also proposes a number of technical improvements, especially for the treatment of the infrared. The main effect of using the newer tracks is that synthetic stellar populations redden more slowly with age. For example, a passively evolving coeval population reaches a color redder than $B-V = 0.8$ within 6 Gyr using the GRV87 model with the old tracks (as does the B83 model), while it takes 8.5 Gyr with the new tracks. This difference has little importance in models in which ellipticals are supposed to be very old (older than ~ 12 Gyr); that is, in almost all of the phenomenological models previously quoted. In fact, the conclusions derived from the number counts in those papers seem to be unchanged by the upgrading of the stellar tracks, although the colors may be somewhat altered. However, it is easy to guess that the effect of using the new tracks will be stronger for models of galaxy formation based on a CDM power spectrum within an $\Omega = 1$ universe, since most galaxies are then predicted to form at low redshift and to be younger than 10 Gyr.

The stellar data which are used here come from Maeder & Meynet (1988) for massive stars and VandenBerg (1985) for low-mass stars. We assume that all stars form with the same initial mass function (IMF). The IMF used is the same as in Paper I and GRV87: it has a piecewise power-law form, $d\mathcal{N}(m_*)/d\ln m_* \propto m_*^{-x}$, with the slope for each segment chosen to provide an approximate fit to the observed IMF in the solar neighborhood (reviewed by Scalo 1986). We assume $x = 1.7$ for the massive stars, $120\ M_\odot > m_* > 2\ M_\odot$, which emit the crucial rest-frame UV fluxes. For the low-mass stars, the slopes are the $x = 1.35$ for $2\ M_\odot > m_* > 1\ M_\odot$ and $x = 0.25$ for $1\ M_\odot > m_* > 0.1\ M_\odot$. In addition to the mass going into visible stars ($m_* > 0.1\ M_\odot$), an equal amount of mass is assumed
to go into invisible objects ($m_* < 0.1\ M_\odot$). This fraction was chosen by GRV87 to provide a fit to the observed M/L ratios of stellar populations in their phenomenological models, and we keep the same fraction here. Finally, we recall that nebular emission is taken into account using the flux of Lyman-continuum photons emitted by O and B stars.

2.5.2. *Internal Extinction*

The spectral evolution models of GRV87 already include a component of extinction by dust within the galaxy, applied uniformly to all the stars. This intrinsic extinction, which we call the "standard" extinction, is computed for the case that the dust and the stars are homogeneously mixed in a plane-parallel layer (see GRV87). The column density of dust is taken as the value it would have for a uniform disk with the same half-mass radius as the stars. The total amount of dust is calculated consistently from the gas mass and metallicity, where the gas mass takes account of star formation and mass loss from stars, and the gas metallicity is calculated using the instantaneous recycling approximation. For bright galaxies, this component of the extinction typically amounts to $A_V \lesssim 0.3$ mag in the face-on case, and $A_V \lesssim 0.5$ mag for an average inclination angle $i = 60°$. Unlike GRV87, who applied this extinction only to spiral galaxies, we apply it to all galaxies that contain gas, including the elliptical galaxies in their early phases.

In addition to this uniform component of internal extinction, which applies equally to all stars, we also consider the possibility that there is an extra component of extinction which applies to massive OB stars only (specifically, stars with main-sequence spectral types earlier than B7, and masses $m_* \gtrsim 4\ M_\odot$). The motivation for this is that such stars are very young and so will mostly still be in the regions of dense gas and dust where they formed. Mochkovitch & Rocca-Volmerange (1984) showed that such an extra component of extinction seems to be necessary to reproduce the UV colors of nearby spiral galaxies. They suggested $\Delta E(B-V) \approx 0.25$ for the extra extinction. This is roughly consistent with the result of Kennicutt (1983), who found from comparing Hα and thermal radio emission that the typical extinction of the star forming regions in normal spiral galaxies is ~ 1.1 mag at the wavelength of Hα, equivalent to $A_V \approx 1.3$ mag. In our models, we adopt a uniform value $\Delta A_V = 1$ mag for the extra extinc-

tion on OB stars. This makes a significant difference to the colors of galaxies undergoing very active star formation.

2.5.3. *Comparison of Results for Different Star Formation Histories*

We ran a grid of models with star formation time scales $\tau_* = (1, 2.5, 3.33, 10)$ Gyr, a model with a constant SFR ($\Psi/M_b = 0.04$ Gyr^{-1}), and models with bursts of duration 0.1 and 1 Gyr. Figure 1 shows the time variation of mass-to-luminosity ratios and $B-V$ colors for these SFR histories, in the cases *with* and *without* additional extinction. It can be seen that the M_b/L_B ratios for the different models span a large range (a factor $\sim$10–100) during the first 2 Gyr, but this narrows to a factor of 5 at an age of 13 Gyr. We included 50% of baryonic dark matter (planets or brown dwarfs) in the IMF, as described above. Such a factor enables the models to reproduce the mass-to-luminosity ratios $M_b/L_B \approx 4$–10 in the central parts of bright galaxies at ages around 10 Gyr. The models in which a short burst of star formation (0.1 or 1 Gyr) is followed by passive stellar evolution show some slight oscillations which are due to the discretization of the stellar tracks (see Charlot & Bruzual 1991 for an analysis). This effect is not the main source of uncertainty, and so we shall keep these curves with their small oscillations. Without the additional extinction, all the $B-V$ colors steadily redden with time. Including the additional extinction changes the mass-to-luminosity ratios and colors of the young/star-forming galaxies and leaves the old/red objects unchanged. In particular, the bluest color now obtained with the standard IMF increases from 0.2 to 0.35. If all the B and V light were due to OB stars, the initial $B-V$ colors would have increased to 0.55. As with time the weight of the OB stars decreases relative to later type stars, the $B-V$ colors first get *bluer* (because of A–F stars), and then *redder* (as the stellar population ages).

This grid of template models is interpolated logarithmically to compute the mass-to-luminosity ratios and colors for each τ_* and $t_{\rm gal} \equiv t - t_*$. (We have checked that a linear interpolation gives similar results.) Finally the luminosity and color distributions are estimated from the distribution $d^3n/d\ln M_b/d\ln(1+z_*)/d\ln\tau_*$.

2.5.4 *Morphological Types and Surface Brightness Distributions*

Our model makes no explicit predictions about morphological type, i.e., whether the stars are distributed in a disk or a spheroid. However, some of the observational data we wish to compare with, such as the Tully-Fisher relation, are for galaxies of a particular morphological type (spiral galaxies, in the case of the Tully-Fisher relation). In such cases, we will recast the observational relations in terms of present color rather than morphological type, using the observed relation between $B-V$ color and morphological type given by de Vaucouleurs (1977).

We also need to make some assumptions about the surface brightness distributions of galaxies, both so that we can compare the models with observed distributions of effective radii seen in projection, and so that we can compute consistent isophotal corrections to the magnitudes used in number counts. The model predicts only the three-dimensional half-mass radius r_* of the stars. We assume that the stars in a galaxy with $v_g > v_{\rm crit}$ are distributed either (1) spherically, so as to give an $r^{1/4}$-law profile in projection (corresponding to elliptical morphology) if $\tau_* < 1$ Gyr; or (2) in a disk, with an exponential profile (corresponding to spiral morphology), if $\tau_* > 1$ Gyr. On the other hand, all of the galaxies with $v_g < v_{\rm crit}$ are assumed to have exponential profiles. The radius r_e containing half the light in projection is then related to the radius r_* of the sphere containing half the stellar mass by $r_e = 0.74 r_*$ for the $r^{1/4}$-law spheroids, and $r_e = r_*$ for the exponential disks. The motivation for relating morphology to star formation time scale in this way is that, in our model, galaxies with small τ_* are predicted at the present day to have the red colors characteristic of ellipticals and S0's, while those with large τ_* are predicted to have the blue colors characteristic of spirals, as shown in Figure 2*d*. Placing the dividing line at $\tau_* = 1$ Gyr produces a relation between morphological type and color of roughly the correct form. Given these assumptions, isophotal corrections to magnitudes are straightforward to compute. Clearly, our model for the surface brightness distribution is very crude, not allowing for bulge components in spiral galaxies, nor disks in S0's, but fortunately the predictions we are

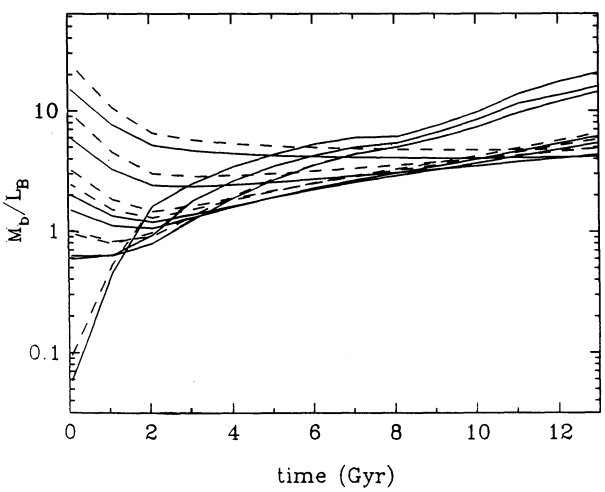

FIG. 1*a*

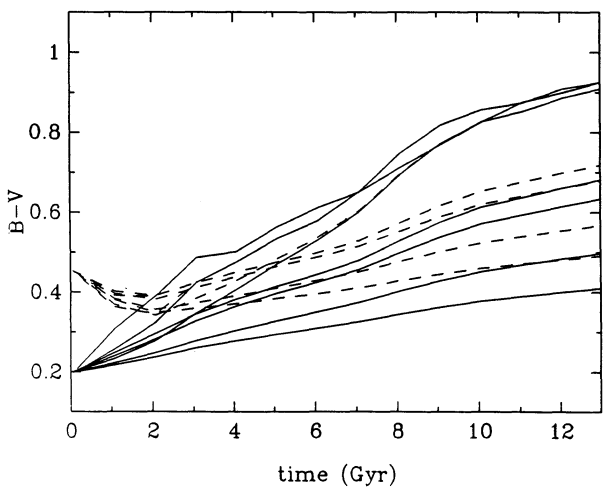

FIG. 1*b*

FIG. 1.—Time variation of (*a*) the baryonic mass-to-luminosity ratios and (*b*) the $B-V$ colors for various SFR histories. The curves are as follows, from top to bottom on the right-hand sides of the panels: bursts of duration 0.1 and 1 Gyr, models with SFR time scales $\tau_* = (1, 2.5, 3.33, 10)$ Gyr, and a constant SFR. Solid and dashed curves show results with and without the extra $\Delta A_V = 1$ mag extinction on OB stars.

interested in are not too sensitive to these assumptions. We note that Guiderdoni & Rocca-Volmerange (1991) also included isophotal corrections in their more phenomenological models, using the same forms for the assumed surface brightness profiles, but assigning the profile type and half-light radius empirically, according to observations of present-day galaxies.

3. PROPERTIES OF NEARBY GALAXIES

In this section, we present the predictions of our model for the properties of galaxies at the present day ($z = 0$), and compare them with observational data on nearby galaxies. We have chosen the following as the parameters for our "standard model": $\sigma_8 = 0.5$, $f_b = 0.06$, $M_{gr}/M_g = 8$, $A_* = 8$, $f_{diss} = 0.05$, moderate mass loss ($v_{crit} = 100$ km s^{-1}, $\gamma = 2$, $f_{*crit} = 1$), and include the extra $\Delta A_V = 1$ mag extinction on OB stars. These parameter values will be assumed below, unless stated otherwise. In comparing with observations, all of the observational data have been corrected to our assumed value of $H_0 = 50$ km s^{-1} Mpc^{-1}.

3.1. *Dependence of Luminosity and Color on Initial Mass*

In Figures 2*a*–2*c*, we show how present luminosities, mass-to-light ratios, and colors depend on the initial baryonic mass, $M_{bi} \equiv M_b$. Figure 2*a* plots the blue luminosity, L_B, against M_b for three different assumptions about mass loss: (1) no mass loss; (2) moderate mass loss ($\gamma = 2, f_{*crit} = 1$); (3) strong mass loss ($\gamma = 2, f_{*crit} = 0.1$). For the case of no mass loss, we find a relation $L_B \propto M_b^{1.2}$. The slope is steeper than 1 because the stellar populations are on average older in lower mass galaxies. This increasing age results from lower mass galaxies both turning on star formation at higher redshift z_* and having shorter star formation time scales τ_* (and ceasing star forma-

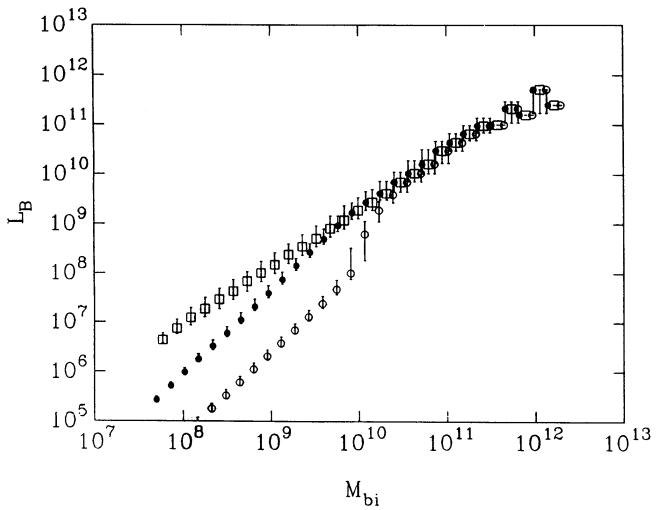

FIG. 2*a*

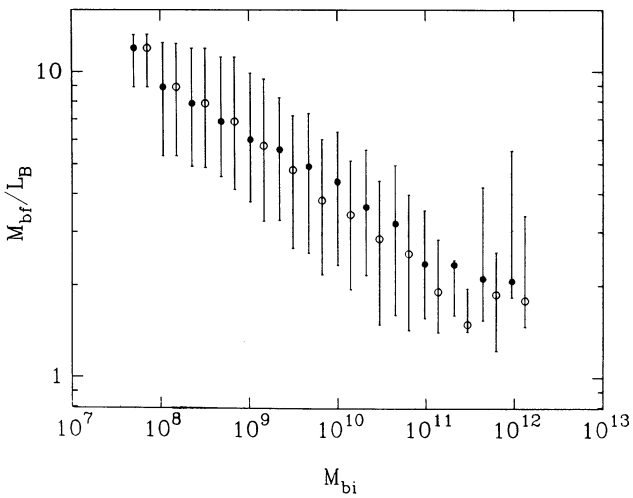

FIG. 2*b*

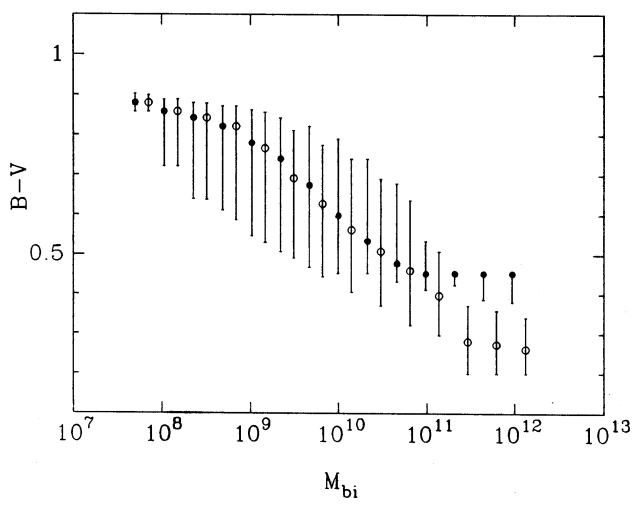

FIG. 2*c*

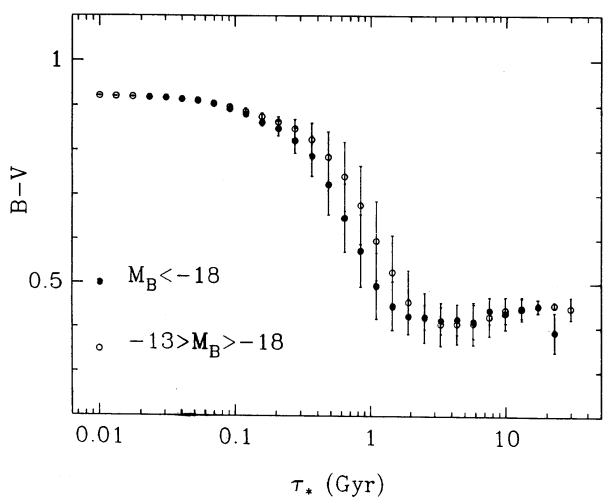

FIG. 2*d*

FIG. 2.—(*a*) Final luminosity vs. initial baryonic mass. The symbols mark the median values, and the bars mark the upper to lower quartile range. *Open squares*: no mass loss. *Filled circles*: moderate mass loss. *Open circles*: strong mass loss. All models include extra extinction on OB stars. (*b*) Final baryonic mass-to-light ratio vs. initial baryonic mass, for moderate mass loss. Symbols mark medians and quartiles. *Open circles*: no extra extinction. *Filled circles*: including extra extinction. (*c*) Final $B-V$ color against initial baryonic mass, with models as in (*b*). (*d*) Final $B-V$ color vs. star formation time scale, shown separately for bright ($\mathcal{M}_B < -18$) and faint ($-13 > \mathcal{M}_B > -18$) galaxies. Symbols mark means and standard deviations.

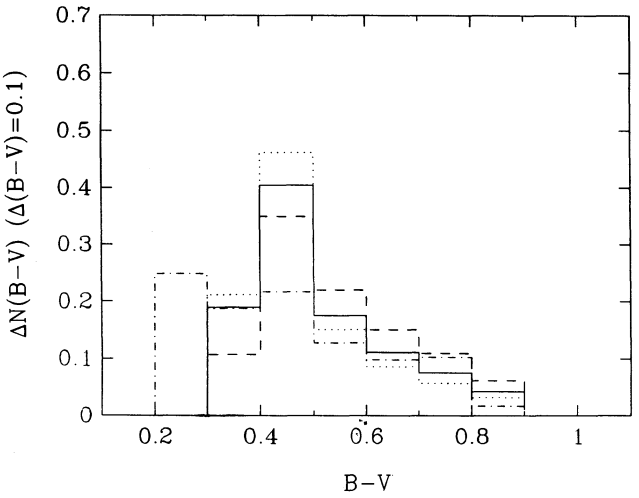

FIG. 3a

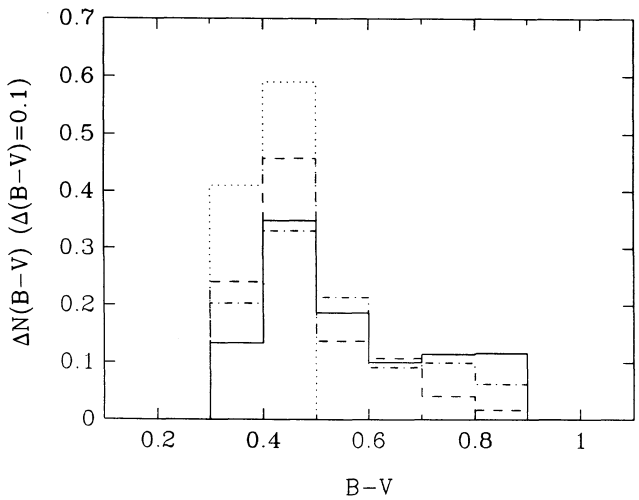

FIG. 3c

FIG. 3.—Distribution of $B-V$ colors (fraction of galaxies per 0.1 mag bin). (*a*) Bright galaxies, $\mathcal{M}_B < -18$. (*b*) Faint galaxies, $-13 > \mathcal{M}_B > -18$. *Solid curve*: standard model, with moderate mass loss and extra extinction. *Dot-dashed curve*: moderate mass loss, without extra extinction. *Dashed curve*: strong mass loss. *Dotted curve*: no mass loss. (*c*) Shows effects of varying σ_8 and star formation history. *Solid curve*: $\sigma_8 = 0.7$. *Dashed curve*: $\sigma_8 = 0.4$. *Dotted curve*: "all Im" SFR history. *Dot-dashed curve*: "all E" SFR history.

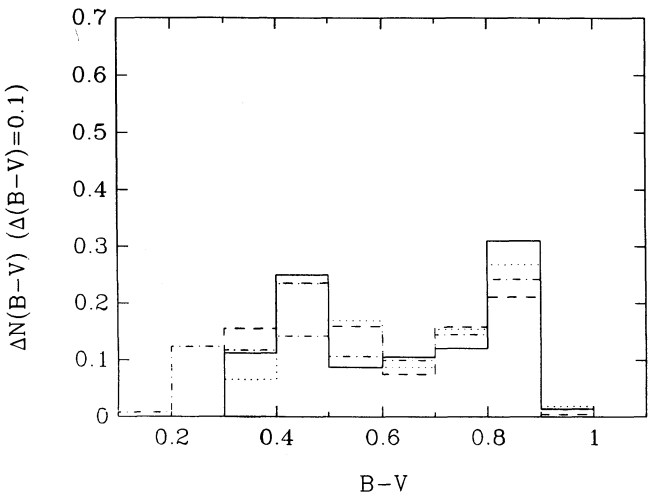

FIG. 3b

tion after mass loss), compared to higher mass galaxies, as was discussed in Paper I. Including mass loss produces a steeper slope, $L_B \propto M_b^{1.7}$ for galaxy masses $M_b \lesssim 10^{10}\ M_\odot$, where mass loss sets in. Figures 2*b* and 2*c* respectively show the dependence on initial baryonic mass of the final baryonic mass-to-light ratio M_{bf}/L_B and the $B-V$ color, for moderate mass loss, with and without the extra extinction. The final baryonic mass $M_{bf} \equiv f_* M_b$ includes the small amount of gas shed by dying stars after the phase of galaxy mass loss. The baryonic mass-to-light ratio and the $B-V$ color both increase with decreasing mass, because of the increasing age of the stellar populations; including the extra extinction, the median value of M_{bf}/L_B varies from ~ 2 at high masses up to 12 at low masses, while that of $B-V$ increases from 0.45 to 0.9 over the same range. Including the extra extinction has a significant effect only for fairly massive galaxies ($M_b \gtrsim 10^{11}\ M_\odot$), which are ~ 1.6 times fainter and 0.2 mag redder when it is included. This is the same trend for young galaxies as noted in Figure 1.

Figure 2*d* shows how the present $B-V$ color depends on the star formation time scale τ_*. The results are shown separately for bright ($\mathcal{M}_B < -18$) and faint ($-13 > \mathcal{M}_B > -18$) galaxies. It can be seen that there is a good correlation, which is not surprising, since the colors depend mainly on τ_* and z_*, the latter tending to correlate with τ_* (as discussed in Paper I). In particular, all galaxies with $\tau_* \lesssim 0.3$ Gyr have very red colors, and all galaxies with $\tau_* \gtrsim 3$ Gyr have very blue colors. Most of the variation in color occurs in the intermediate range, $0.3 \lesssim \tau_* \lesssim 3$ Gyr, and here there is a separation between high- and low-luminosity galaxies. Note that in most phenomenological models, all galaxies of a given morphological type are assumed to form at the same redshift, and to have identical star formation histories so that there is an *exact* correlation between $B-V$ and star formation time scale.

3.2. *Color Distribution*

Figures 3*a* and 3*b* show the present $B-V$ color distributions in a given volume for bright ($\mathcal{M}_B < -18$) and faint ($-13 > \mathcal{M}_B > -18$) galaxies, respectively. Note that mass loss sets in at $\mathcal{M}_B \gtrsim -18$. The strong tendency, which these figures show, for the more luminous galaxies to be bluer reflects the trend of color with mass already discussed and is a basic feature of our model. Our assumption that star formation in a galaxy begins only when the surrounding group collapses means in the context of the CDM model that most star formation is shifted to quite low redshifts ($z \lesssim 1$). In particular, many massive galaxies are predicted to be very actively forming stars at the present day, having only recently turned on star formation. These galaxies are very blue. On the other hand, most low-mass galaxies begin star formation at $z_* \gtrsim 1$, convert gas into stars on quite a short time scale, and then stop forming stars when they lose their remaining gas. These galaxies are by now very red. However, since there is a distribution in z_*-values, some low-mass galaxies turn on star formation fairly recently, producing the second, blue, peak in Figure 3*b*. These points are illustrated in Figures 4*a* and 4*b*, which show the distributions of z_* and τ_* for bright and faint galaxies separately. The distribution of star formation time scales of bright galaxies shown in Figure 4*b* is similar to the distribution of gas depletion time scales of normal spirals found observationally by Kennicutt (1983), for large τ_*. (It is not possible to make a more precise

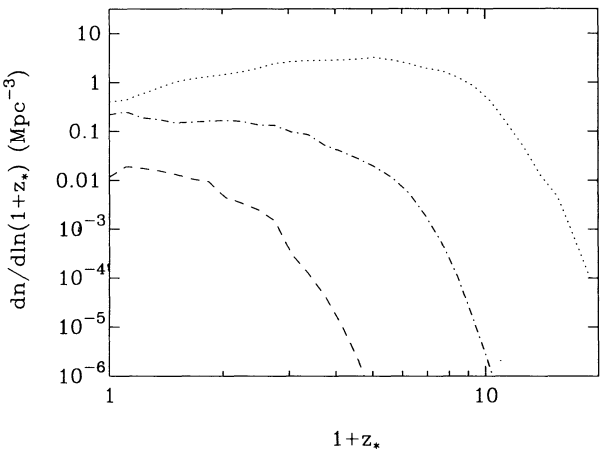

FIG. 4a

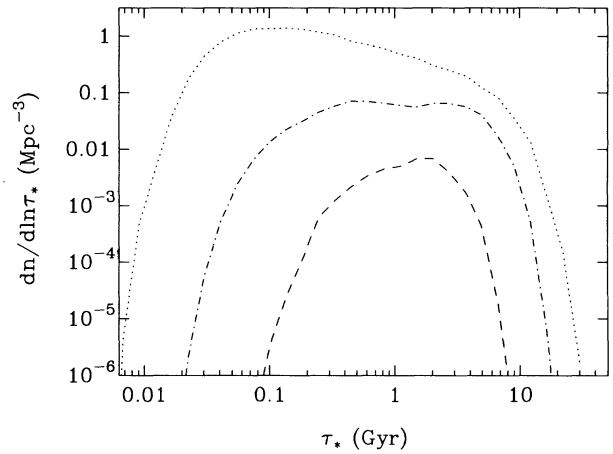

FIG. 4b

FIG. 4.—Distribution of (*a*) star formation turn-on redshift and (*b*) star formation time scale, for bright ($\mathcal{M}_B < -18$; *dashed curve*), faint ($-13 > \mathcal{M}_B > -18$; *dot-dashed curve*), and very faint ($\mathcal{M}_B > -13$; *dotted curve*) galaxies.

comparison with Kennicutt's data, since the way his sample is selected means that it is not representative of the entire Hubble sequence.)

Figures 3*a* and 3*b* also show the effects on the color distributions of varying the assumptions about extinction and mass loss. Including the extra extinction on OB stars has the effect of removing the extreme blue objects with $0.2 \lesssim B-V \lesssim 0.3$, displacing them into a peak at $0.4 \lesssim B-V \lesssim 0.5$, while varying the amount of mass loss has relatively little effect on the colors. In this paper, we find somewhat bluer colors for bright galaxies than we did in Paper I, even though those models did not include any extinction. This is because of the new stellar tracks used. For our standard model, the fraction of bright galaxies with colors redder than $B-V > 0.8$ is only $\sim 4\%$. This small fraction of red galaxies is a serious problem for the model, since observations show that 20%–30% of bright galaxies are ellipticals or S0s (see, for instance, the discussions in Paper I or in Guiderdoni & Rocca-Volmerange 1990), which acording to de Vaucouleurs (1977) have colors $B-V > 0.8$. For the faint galaxies, the fraction with $B-V > 0.8$ increases to $\sim 30\%$ in our standard model. The faint galaxies cover the whole range of colors $0.3 < B-V < 1.0$, so qualitatively we can account for the presence of both dwarf spheroidals and star-forming irregulars.

Figure 3*c* shows the effects on the colors of bright galaxies of varying the amplitude σ_8 of the CDM power spectrum down to 0.4 and up to 0.7. The fraction of red ($B-V > 0.8$) galaxies is fairly sensitive to σ_8, varying from 2% up to 12% as the amplitude is increased. This is because a larger amplitude results in earlier galaxy formation, and thus older galaxies by the present day. Figure 3*c* also shows the effect of varying the star formation history while keeping z_* for each galaxy the same as in the standard model: the extreme possibilities we consider are for the star formation to all occur in a 0.1 Gyr burst ("all E"), or for the star formation rate to be constant at 0.04 Gyr^{-1} per unit baryonic mass ("all Im"). The "all Im" model makes all the galaxies very blue ($B-V < 0.5$), while the "all E" model does not differ that much from our standard model. These models correspond roughly to the extreme range in the values of τ_* for galaxies in our model and illustrate that modest changes in the value of A_* assumed (say, by a factor of 2 either way) would not much change our predictions (see also Paper I). In particular, this exercise shows that the deficiency of very red galaxies results from the distribution of z_* values and cannot be remedied by changing the distribution of τ_*.

In Paper I, we attempted to make a direct observational comparison with the predicted color distribution in a volume-limited sample. However, with existing observational data, a detailed comparison of predicted and observed color distributions is best made using galaxy number counts, and so we defer this to the next section.

3.3. *Radii and Surface Brightnesses*

Here we consider the radii and surface brightnesses of the luminous stellar components of galaxies. Figure 5*a* shows the dependence of the three-dimensional half-mass radius of the baryons on the baryonic mass, both before and after mass loss. Even with the assumption of a constant collapse factor $f_{\rm diss}$, there is a spread in radii at a given mass because of the spread in halo densities. Before mass loss, the radius is roughly fitted by $r_{*i} \propto M_{bi}^{0.4}$ over the range $10^8 \lesssim M_b \lesssim 3 \times 10^{11}\ M_\odot$. After mass loss, the slope for $M_b \lesssim 10^{10}\ M_\odot$ is reduced to $r_{*f} \propto M_{bf}^{0.2}$.

Figure 5*b* shows the resulting relation between the effective surface brightness $\langle\mu\rangle_e$ and absolute magnitude $\mathcal{M}_B$ for present-day galaxies. (We will use the notation Σ for the surface brightness measured on a linear scale, and $\mu \equiv -2.5$ log Σ + const for the surface brightness expressed in mag arcsec^{-2}.) The effective surface brightness is defined to be the mean surface brightness within the radius r_e containing half of the light when seen in projection; r_e is related to r_* as described in § 2. We have plotted the model predictions separately for the color ranges $B-V > 0.8$, $0.8 > B-V > 0.6$ and $B-V < 0.6$, which observationally correspond to the morphological types E-S0, Sa-Sb, and Sc-Sd-Im, respectively, according to de Vaucouleurs (1977). The models predict that the bluer galaxies should have slightly lower surface brightness than red galaxies, at a given blue luminosity. To compare with the models, we have plotted the observational $\langle\mu\rangle_e$-$\mathcal{M}_B$ relation for elliptical galaxies found by Binggeli, Sandage, & Tarenghi (1984). For the fainter ellipticals ($\mathcal{M}_B \gtrsim -19$), this is based entirely on data from the Virgo cluster and the Local Group. We have shown only the low surface brightness (LSB) branch of dwarf ellipticals, and omitted the high surface brightness dwarf ellip-

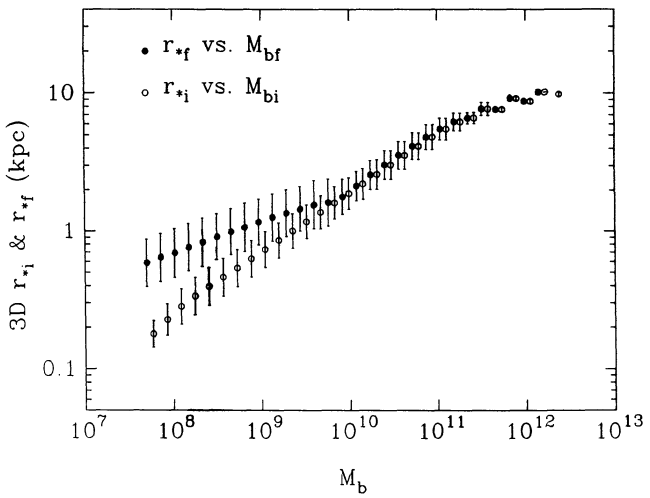

FIG. 5a

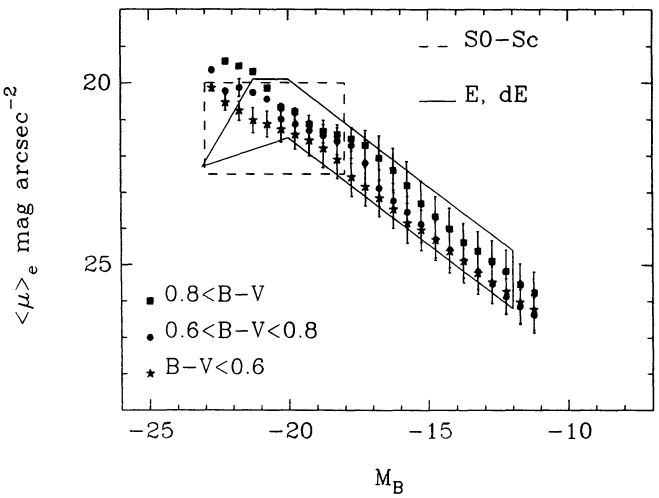

FIG. 5b

FIG. 5.—(*a*) Relation of three-dimensional half-mass radius r_* of baryonic core to baryonic mass. Symbols mark means and standard deviations for models. Figure shows both the initial radius vs. initial baryonic mass, and the final radius, after mass loss, vs. final baryonic mass. (*b*) Relation between mean surface brightness $\langle\mu\rangle_e$ within projected half-light radius and absolute magnitude. Symbols mark means and standard deviations for models, for the color ranges indicated. The boxes show the observed region for ellipticals, from Binggeli et al. (1984), and the observed region for bright spiral's and S0's, from Sandage (1983).

ticals of the M32 type, which appear to be much less numerous. Published data on the $\langle\mu\rangle_e$-$\mathcal{M}_B$ relation for spiral and dwarf irregular galaxies are less complete, although they indicate similar behavior to that found for the ellipticals. For bright spirals ($\mathcal{M}_B \lesssim -18$), we have plotted the data of Sandage (1983). For fainter star-forming systems, we note the result of Binggeli (1985), who finds that dE and Im galaxies in the Virgo cluster with $\mathcal{M}_B \gtrsim -17$ follow similar relations between the mean surface brightness within the $\mu_B \approx 25.5$ mag arcsec^{-2} isophote and magnitude. Since both types are well fitted by exponential surface brightness profiles in this range, this implies that their $\langle\mu\rangle_e$-$\mathcal{M}_B$ relations should also be similar. As a caveat, we note the claim by Impey, Bothun, & Malin (1988) that the correlation between surface brightness and luminosity breaks down at $\mathcal{M}_B \gtrsim -16$; they find dwarf galaxies in the Virgo cluster which have even lower surface brightnesses (by 1–2 mag arcsec^{-2}) than those in the Binggeli et al. sample at the same absolute magnitude.

We have attempted to fit the Binggeli et al. surface brightness-magnitude relation for E's and dE's with our predicted relation for red ($B-V > 0.8$) galaxies, with the dissipative collapse factor $f_{\rm diss}$ as our one adjustable parameter. It can be seen that the final fit with $f_{\rm diss} = 0.05$ is quite good, except for ellipticals brighter than $\mathcal{M}_B \lesssim -21$, for which the models predict a continuing increase of surface brightness with increasing luminosity, while the observations actually show a decline. This discrepancy may indicate the breakdown of our assumption that $f_{\rm diss}$ is the same for all galaxies. Alternatively, it may result from the formation of massive ellipticals by merging of disk galaxies, a process which is not included in our models. The bluer ($B-V < 0.8$), bright ($\mathcal{M}_B \lesssim -18$) galaxies are predicted to occupy roughly the same region of the $\langle\mu\rangle_e - \mathcal{M}_B$ plane as observed normal S's and S0's, although the observations show a flatter trend, with more scatter, compared to the predictions. This could be influenced by the presence of a bulge in real disk galaxies, while our modeling assumed a pure disk component. The fact that the surface brightness—luminosity relation predicted by the models is close to a single power law over the range plotted is somewhat fortuitous—without mass loss, the relation would be flatter at low luminosities.

3.4. *Dependence of Circular Velocity and Velocity Dispersion on Luminosity*

Figure 6*a* shows the dependence of the circular velocity V_c of the halo in which a galaxy formed on the final mass of the baryonic core, after mass loss. We have taken the circular velocity V_c equal to the halo velocity dispersion v_g. The slope of the relation steepens from $V_c \propto M_b^{0.2}$ at low masses, $10^8 \lesssim M_b \lesssim 10^{10}\ M_\odot$, to $V_c \propto M_b^{0.3}$ at higher masses, $10^{10} \lesssim M_B \lesssim 10^{12}\ M_\odot$. We can roughly estimate the effect of the baryons' self-gravity on the circular velocity V_{c*} within the baryon half-mass radius r_* as $V_{c*}^2 = V_c^2 + GM_b/2r_*$, and this is also plotted in the figure. This is seen to produce a 40% increase in the circular velocity at high masses, but very little effect at low masses, where mass loss reduces the self-gravity of the baryons. Since our estimate of V_{c*} is rather uncertain, we prefer in what follows to work in terms of the *halo* circular velocity V_c, which is better defined.

In Figure 6*b*, we show the variation of the halo circular velocity V_c with the blue luminosity. The predictions are shown separately for the same three color ranges as in Figure 5*b*. It can be seen that the relation for blue galaxies is displaced toward lower circular velocities and/or higher blue luminosities relative to that for red galaxies. This results from the fact that, at a given mass, a lower density halo has a lower circular velocity, and also, on average, has smaller z_* and larger τ_*, producing a galaxy with a younger stellar population. To compare with the predictions, we have plotted the Tully-Fisher (TF) relation for spiral galaxies from Kraan-Korteweg, Cameron, & Tamman (1988), assuming that V_c is half the H I 21 cm linewidth. This assumption is based on the observed flatness of spiral galaxy rotation curves in their outer parts. These data, and those on the surface brightness, are consistent with a Virgo Cluster distance of $\sim$22 Mpc, and with our assumed Hubble constant $H_0 = 50$ km s^{-1} Mpc^{-1}. This observed TF relation, with a slope $L_B \propto V_c^{2.7}$ is steeper than the predicted relations for galaxies of a given color, which have

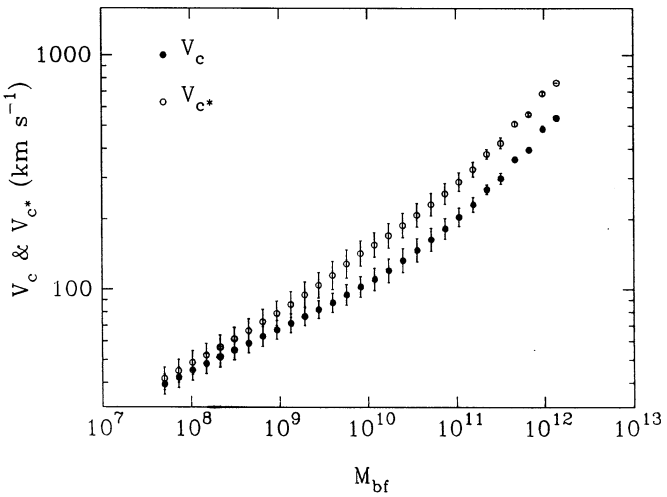

FIG. 6a

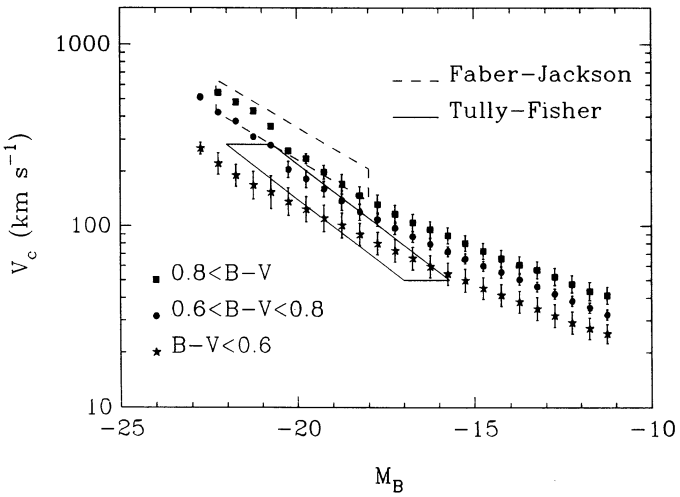

FIG. 6b

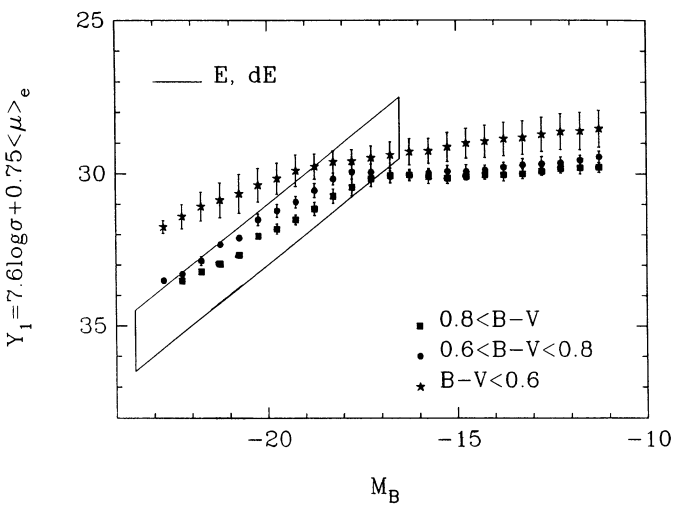

FIG. 6c

FIG. 6.—(*a*) Relation between halo circular velocity and baryonic mass. Symbols mark means and standard deviations for models. Filled symbols show circular velocity V_c of halo, open symbols show an estimate of the circular velocity V_{c*} at the half-mass radius of the baryons. (*b*) Relation between halo circular velocity V_c and absolute magnitude. Symbols mark means and standard deviations for models, for color ranges indicated. Boxes show the observed Tully-Fisher relation for spiral galaxies, from Kraan-Korteweg et al. (1988), and the Faber-Jackson relation for ellipticals, from Dressler et al. (1987). For the ellipticals, we have assumed $V_c = (3)^{1/2}\sigma_*$. (*c*) Projection of galaxy properties perpendicular to observed "fundamental plane" for ellipticals. Symbols show models as before, and box shows region occupied by observational data on ellipticals from Faber et al. (1989) and Nieto et al. (1990).

$L_B \propto V_c^4$ over the range $-12 \gtrsim \mathcal{M}_B \gtrsim -21$, although it spans the range between our two bluest classes, which correspond by color to SaSb's and Sc-Sd's. However, Rubin et al. (1985) find that the TF relations for spirals separated by morphological type do have slopes close to $L_B \propto V_c^4$ and that Sc's are brighter than Sa's at the same V_c by $\Delta\mathcal{M}_B \approx 2$ mag. Our predictions agree rather well with these observational results.

We have also plotted the Faber-Jackson (FJ) $L_B - \sigma_*$ relation for ellipticals from Dressler et al. (1987), with a slope $L_B \propto \sigma_*^{3.5}$. In the case of ellipticals, the relation between the measured one-dimensional velocity dispersion σ_* of the stars and the circular velocity V_c of the surrounding dark halo is much more uncertain, observationally and theoretically, than the relation between measured and halo circular velocities for spirals. For simplicity, we have assumed a constant ratio V_c/σ_*. If the stars were a non–self-gravitating test population with density profile $\rho_* \propto r^{-3}$ within a singular isothermal halo ($\rho_H \propto r^{-2}$), one would have $V_c/\sigma_* = 3^{1/2}$. This value was used by Gunn (1982) and Blumenthal et al. (1984) in converting from observed to halo properties of ellipticals, and the observational data presented by Fall (1987) indicates that this assumed ratio may not be too bad, even though the self-gravity of the stars probably is important in the central regions where σ_* is measured. We will use $V_c = (3)^{1/2}\sigma_*$ in what follows, but the results should only be regarded as illustrative, for the reasons given. In Figure 6*b*, we see that for the reddest color class in the models, which corresponds to E-S0's, the predicted $V_c - L_B$ relation is slightly steeper than that inferred from observations in the same luminosity range.

For observed elliptical galaxies, a tighter correlation of velocity dispersion with other properties is found to be given by a three parameter $L - \sigma_* - \langle\Sigma\rangle_e$ relation, rather than the two parameter $L - \sigma_*$ relation. Elliptical galaxies are found to be concentrated around a "fundamental plane" of the form $L_B \propto \sigma_*^x \langle\Sigma\rangle_e^y$, with exponents $x = 2.65$, $y = -0.65$ according to Dressler et al. (1987), and $x = 3.45$, $y = -0.86$ according to Djorgovski & Davis (1987). Following Nieto et al. (1990), we adopt an average of these two determinations, with $x = 3.05$ and $y = -0.75$, leading to a fundamental plane relation $\mathcal{M}_B = -Y_1 + \text{const}$, where $Y_1 \equiv 7.61 \log \sigma_* + 0.75\langle\mu\rangle_e$. Figure 6*c* shows the distribution of galaxies in the $Y_1 - \mathcal{M}_B$ plane, effectively viewing the fundamental plane edge-on. The figure shows the model predictions for various colors, again calculated assuming $\sigma_* = V_c/3^{1/2}$, and the region occupied by observed ellipticals, according to data from Faber et al. (1989) and Nieto et al. (1990). (We prefer to use the fundamental plane to compare models and data, rather than the essentially equivalent D_n-σ_* relation, because the theoretical interpretation for the former is rather more obvious.) Given our assumptions, the redder galaxies are predicted to occupy the same region of the diagram as observed ellipticals, but the same caveats about relating σ_* to V_c must be borne in mind.

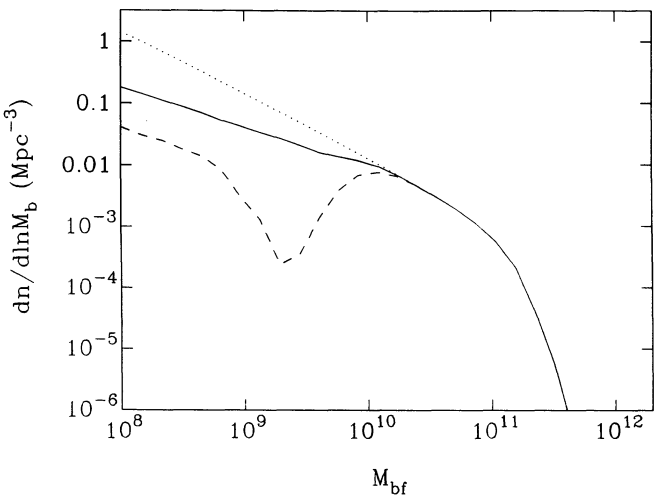

FIG. 7.—Distribution of final baryonic masses of galaxies, for various assumptions about mass loss: *Dotted line*: no mass loss. *Solid line*: moderate mass loss. *Dashed line*: strong mass loss.

3.5. *Galaxy Luminosity Function*

We now come to the present-day galaxy luminosity function, a crucial quantity in our models. Figure 7 shows the predicted final baryonic mass distributions, for the same three assumptions about mass loss as in Figure 2*a*, i.e., no mass loss, moderate mass loss, and strong mass loss. The slope of this relation at low masses is $dn/dM_b \propto M_b^{-2}$ before mass loss, and $dn/dM_b \propto M_b^{-1.65}$ after mass loss. In the case of strong mass loss, the discontinuity in f_* at $v_g = v_{\rm crit}$ produces a strong dip in the mass function around $M_b \sim 2 \times 10^9\, M_\odot$.

Figure 8*a* shows the predicted present luminosity functions (LFs), for the same assumptions about mass loss. The faint-end slope is approximately $dn/dL \propto L^{-1.95}$ without mass loss, and $dn/dL \propto L^{-1.60}$ including mass loss. Note that the slope of the luminosity function is not exactly the same as that of the mass function, since there is a weak trend of increasing baryonic mass-to-light ratio with decreasing mass, as shown in Figure 2*b*. In the case of strong mass loss, the dip in the mass function is smoothed out into a flat region in the luminosity function in the range $-15 \gtrsim \mathcal{M}_B \gtrsim -19$, as a result of the large dispersion in the luminosity at a given mass.

Figure 8*a* also shows some observational determinations of the present luminosity function, presented in the form of Schechter function fits, where the Schechter function has the form $dn/dL = (\phi_*/L_*)(L/L_*)^\alpha \exp(-L/L_*)$. Most relevant for our comparison is the field luminosity function, for which the most recent determination is that of Loveday et al. (1992), which we have plotted. They find a fit with $\alpha = -0.95 \pm 0.13$, $\mathcal{M}_{B*} = -21.18$ and $\phi_* = 1.55 \times 10^{-3}$ Mpc^{-3}, over the magnitude range $-17 \gtrsim \mathcal{M}_B \gtrsim -23$. The form of the observed field LF at lower luminosities has not been accurately determined, although Binggeli, Tarenghi, & Sandage (1990) have estimated a faint end slope $\alpha \sim -1$ down to $\mathcal{M}_B \approx -14$ for nearby field galaxies, from the ratio of dwarf to giant galaxies seen on deep photographic plates. This estimate is, however, fairly rough, as they do not have redshifts for most of the low-luminosity galaxies.

It is also of interest to compare our predictions with the shape of the luminosity functions found in galaxy clusters. Most estimates of the field LF are based on measuring redshifts for samples of galaxies limited by apparent magnitude, but this method may be biased against low-luminosity galaxies, especially if they have low surface brightness. Samples of galaxies drawn from galaxy clusters should come closer to being volume-limited samples, and avoid the need to measure redshifts. Clusters might therefore provide a fairer estimate of the shape of the luminosity function at the faint end, although it is also possible that there are real differences between the shapes of cluster and field LFs. In Figure 8*a*, we have plotted the luminosity function for the Virgo Cluster found by Sandage, Binggeli, & Tamman (1985), with parameters $\alpha = -1.3$ and $\mathcal{M}_B = -21.4$, down to $\mathcal{M}_B \lesssim -12$. This has been arbitrarily normalized to match the Loveday et al. field LF at the bright end. The Virgo Cluster LF is seen to be steeper at the faint end than the field LF. This could be a result of the different surface brightness thresholds used, $\langle\mu\rangle_e \approx 25.5$ mag arcsec^{-2} for Sandage et al. and $\langle\mu\rangle_e \approx 24$ mag arcsec^{-2} for Loveday et al. (As before, $\langle\mu\rangle_e$ is defined as the mean surface brightness within the half-light radius.) Ferguson & Sandage (1991) find similarly steep slopes, $\alpha \approx -1.3 \rightarrow -1.6$, in several other groups and clusters, when they include galaxies down to $\mathcal{M}_B \lesssim -13$. Impey, Bothun, & Malin (1988) have studied Virgo down to an even fainter limiting surface brightness, $\mu_B \approx 27$ mag arcsec^{-2}, and find galaxies not included in Sandage et al.'s sample. Based on this, Bothun, Impey, & Malin (1991) apply an incompleteness correction which leads to faint-end slopes $\alpha \approx 1.6$ for Virgo and Fornax. It is not yet clear whether similar effects apply to the field LF.

In fact, using the galaxy radii predicted by our models, we can calculate what the effect will be of only selecting galaxies above some minimum surface brightness. Figure 8*b* shows the predicted luminosity function for our standard model for the thresholds $\langle\mu\rangle_e = (22, 23, 24)$ mag arcsec^{-2}. The effect of imposing a surface brightness criterion is to produce a steep decline in the luminosity function below some luminosity, rather than a general flattening of the faint-end slope. For the threshold $\langle\mu\rangle_e \approx 24$ mag arcsec^{-2} appropriate for the Loveday et al. field galaxy sample, the effect on the luminosity function brighter than $\mathcal{M}_B \lesssim -17$ is very small.

Comparing with observations, we see that our models give a reasonable fit to the field LF at the bright end ($\mathcal{M}_B \lesssim -20$), both in amplitude and in shape. As was noted in Paper I, the bright end cutoff results from our cooling criterion, equation (6), while the amplitude depends on our assumption that star formation in a galaxy only turns on when the surrounding group collapses (eq. [7]), which provides a form of "natural biasing." If we had assumed that star formation began as soon as the galaxy halo itself collapsed, we would have predicted a number density of galaxies ~ 4 times larger at $L \sim L_*$. For fainter galaxies, the predicted LF exceeds that found in the field, by an amount which depends on mass loss. For our standard model, with moderate mass loss, the faint-end slope is $\alpha \approx -1.6$, much steeper than found by Loveday et al., and predicting 5–10 times more galaxies at $\mathcal{M}_B = -17$ than are observed (even allowing for a factor 2 statistical uncertainty in the observations). With strong mass loss, the average slope in the range $-13 \lesssim \mathcal{M}_B \lesssim -20$ is reduced to $\alpha \approx -1.3$, less discrepant with the field LF, and in quite good agreement with Sandage et al.'s Virgo Cluster LF. However, the strong mass-loss model predicts too few galaxies in the faint counts, as will be discussed in § 4.1.

Is it possible to reconcile the field LF predicted by our standard model with that observed by Loveday et al.? As we have seen, a simple surface brightness threshold in the selection of

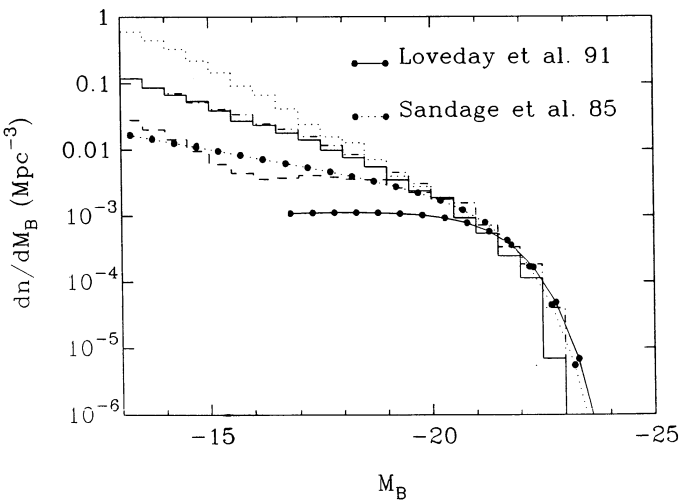

FIG. 8*a*

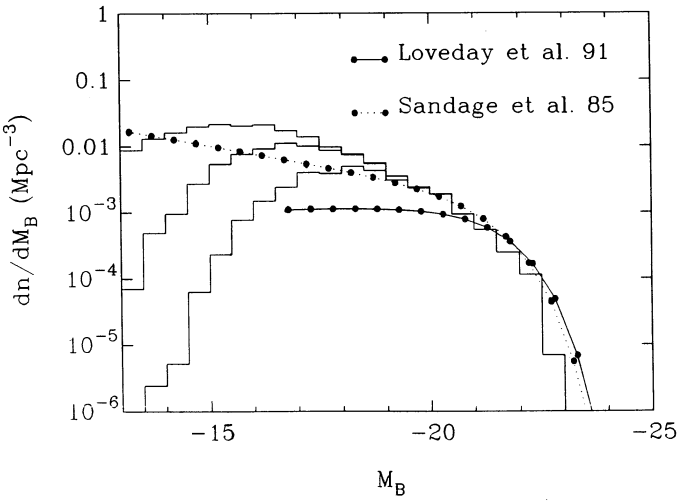

FIG. 8*b*

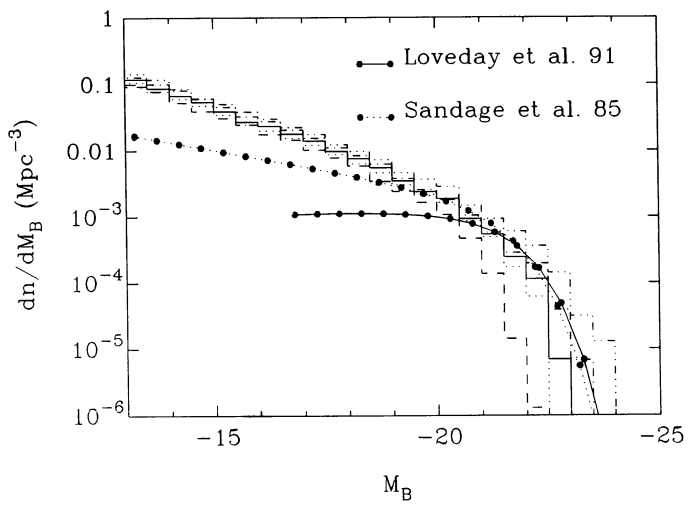

FIG. 8*c*

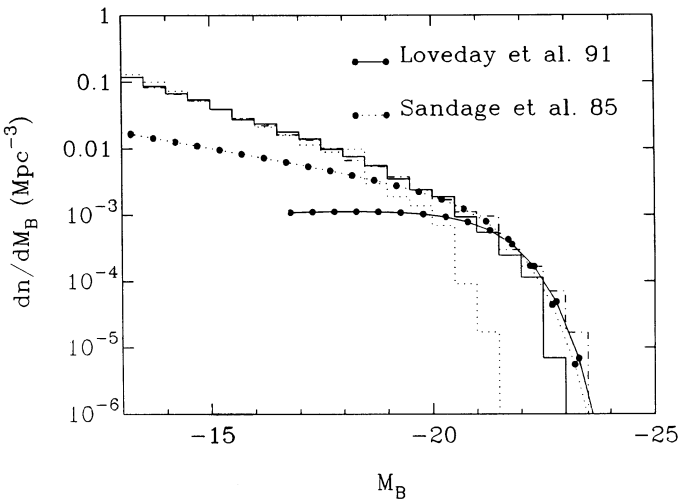

FIG. 8*d*

FIG. 8.—Present galaxy luminosity function. (*a*) Total number density of galaxies per unit absolute magnitude, $dn/d\mathcal{M}_B$. Histograms show predicted distributions for various assumptions about mass loss. *Dotted histogram*: no mass loss. *Solid histogram*: moderate mass loss with additional extinction (our standard model). *Dot-dashed histogram*: moderate mass loss without additional extinction. *Dashed histogram*: strong mass loss. Smooth curves show Schechter function fits to observed luminosity functions: *Solid curve*: Loveday et al. (1991) fit to field luminosity function. *Dotted curve*: Sandage et al. (1985) fit to Virgo Cluster luminosity function, normalized to agree with Loveday et al. at bright end. (*b*) Predicted luminosity functions including effects of surface brightness threshold. Histograms show predictions for $\langle\mu\rangle_e$ brighter than (22, 23, 24) mag arcsec^{-2}, respectively. Smooth curves are same observational LFs as in (*a*). (*c*) shows effects of varying σ_8 and f_b. *Solid histogram*: $\sigma_8 = 0.5$, $f_b = 0.06$ (standard model). *Dashed histogram*: $\sigma_8 = 0.5$, $f_b = 0.04$. *Dash-dot-dot-dot histogram*: $\sigma_8 = 0.5$, $f_b = 0.09$. Dotted histogram: $\sigma_8 = 0.4$, $f_b = 0.06$. *Dot-dashed histogram*: $\sigma_8 = 0.7$, $f_b = 0.06$. (*d*) shows effects of varying the star formation history, while keeping z_* fixed. *Solid histogram*: standard model. *Dotted histogram*: "all Im." *Dot-dash*: "all E."

the original galaxy sample does not seem sufficient to account for the difference. Perhaps there are additional observational biases causing incompleteness at the faint end, such as the difficulty of measuring redshifts for low surface brightness, non–star-forming galaxies. Alternatively, our model assumptions for computing baryonic radii r_* may need to be modified. If low-luminosity galaxies have larger radii than we assume, perhaps due to $f_{\rm diss}$ increasing with decreasing mass, or due to there being a significant *spread* in $f_{\rm diss}$ at a given mass (as tidal torques might suggest for disks), then many of them could still be hiding as an undetected low surface brightness population.

Finally, we consider the effect on the luminosity function of varying some of the other model parameters. In Figure 8*c* we vary σ_8, the amplitude of the CDM power spectrum, and f_b, the baryonic fraction. Increasing σ_8 increases the number density at the bright end, and vice versa, but the effect is not that large for $0.4 < \sigma_8 < 0.7$. There is a larger effect from varying the baryon fraction in the range $0.04 < f_b < 0.09$, with the luminosity of the bright-end cutoff varying roughly as f_b^2. We note that the "best-fit" value of f_b is dependent on the parameters in the cooling criterion, which depend somewhat on the assumed halo density profile. Changes in these parameters can, to some degree, be compensated in their effects on the luminosity function by changes in f_b. In Figure 8*d* we vary the star formation history from our standard model, while keeping the same turn-on redshifts z_*. As in Figure 3*c*, we consider two extreme possibilities, a 0.1 Gyr burst, called the "all E" model and a 0.04 Gyr^{-1} constant SFR, called the "all Im" model. These illustrate how changing the SFR only affects the bright end of the LF, but leaves the faint-end slope unchanged.

4. PROPERTIES OF HIGH-REDSHIFT GALAXIES

In this section, we use our model to compute how the properties of galaxies would have evolved from early times, and compare with the observational data constraining the form of the luminosity and color distributions at high redshifts. We adopt the same standard model as in the previous section.

4.1. *Galaxy Number Counts*

Historically, galaxy number counts down to faint magnitudes have provided the main observational constraint on the evolution of the galaxy population at high redshift. The number of galaxies per unit solid angle in some range of apparent magnitude dm and redshift dz is given by

$$d^2N(m, z) = \frac{dn}{d\mathcal{M}}[\mathcal{M}(m, z), t(z)] \frac{dV(z)}{dz} dm\, dz\ , \qquad (13)$$

where dV/dz is the comoving volume per unit redshift per unit solid angle (e.g., Weinberg 1972), $dn/d\mathcal{M}$ is the number of galaxies per unit comoving volume per unit absolute magnitude $\mathcal{M}$ at redshift z, and the absolute and apparent magnitudes are related by $\mathcal{M}(m, z) = m - DM(z)$, $DM(z)$ being the bolometric distance modulus. The absolute magnitude in this equation is calculated by integrating over the galaxy spectrum after redshifting to the observer's frame, weighted by the response function for that magnitude system, and so corresponds to a redshift-dependent bandpass in the galaxy rest frame. In this way, both k- and e-corrections are automatically included in the calculation. The predicted number of galaxies per unit solid angle, dN/dm, is obtained from equation (13) by integrating over all redshifts. Some of the observational data give counts as a function of isophotal rather than total magnitudes. Therefore, where appropriate, we compute isophotal magnitudes from the models, by integrating over the assumed surface brightness profile out to the limiting isophote, using the surface brightness distributions described in § 2.5, and theoretical half-light radii r_e. The isophotal corrections computed in this way are very similar to those calculated using the more empirical procedure of Guiderdoni & Rocca-Volmerange (1991), since our predicted $r_e - \mathcal{M}_B$ relation agrees well with the observational one used by the latter, except for the brightest galaxies.

In Figure 9, we show the predictions for the number counts in the B_J band. (We will use the notation B_J for the J^+ magnitude in the system of Kron (1980) and Koo (1985), and R_F for the F^+ magnitude). Figure 9*a* shows the counts as a function of total magnitude for various assumptions about mass loss and internal extinction. At brighter magnitudes, $B_J \lesssim 24$, the model counts are dominated by fairly massive galaxies, $M_b \gtrsim 10^{10}$ $M_\odot$, for which mass loss is unimportant. However, the contribution of these galaxies falls off at faint magnitudes, $B_J \gtrsim 24$, because they only begin forming stars at quite low redshifts, $z_* \lesssim 1$. For $B_J \gtrsim 24$, the counts are dominated by the low-mass dwarf galaxies, $M_b \lesssim 10^{10}$ $M_\odot$, and become sensitive to the assumptions about mass loss for these systems. We show the effects on the predictions of using isophotal rather than total magnitudes in Figure 9*b*, for various isophotal thresholds. For deep thresholds, such as the value $\mu_{B_J} = 28.7$ mag arcsec^{-2} used by Tyson (1988), there is little difference from using total magnitudes. Figures 9*a* and 9*b* also show the published observational data on number counts, compiled and reduced to a single photometric system as described in Guiderdoni & Rocca-Volmerange (1990a, 1991). Our standard model, with moderate mass loss and including the extra extinction on OB stars, is seen to provide a reasonable fit, and in particular reproduces the large number of faint galaxies seen in the deep counts of Tyson (1988) and Lilly, Cowie, & Gardner (1990). We note that Tyson and Lilly et al. find very similar results for the faint counts, despite different analysis techniques, and the much better seeing and pixel sampling in the data of Lilly et al. as compared to Tyson. The counts are somewhat excessive compared to the observations at brighter magnitudes, $15 \lesssim B_J \lesssim 20$, because our predicted current LF has twice as many galaxies as observed at $\mathcal{M}_B \approx -20$. The slope in this range is correct, however. For no mass loss, the fit is almost as good as for moderate mass loss. On the other hand, the model with strong mass loss, which gave a better fit to the present luminosity function, predicts far too few galaxies in the faint counts, by about a factor 6 at $B_J = 27$.

In Figure 10, we display the B_J-band number counts in a different way, with a power-law relation $dN/dm \propto 10^{0.45m}$ divided out. This representation serves to emphasize the discrepancies in detail which still exist between different observational data sets, and between the models and the observations. In particular, it is interesting to compare with the recent number count data at bright magnitudes, $15 \lesssim B_J \lesssim 20$, from Maddox et al. (1990a, b), which have very small statistical errors. The more traditional models of luminosity function evolution, such as that of Guiderdoni & Rocca-Volmerange (1990a, b), in which galaxies are all assumed to turn on star formation at high redshifts ($z \gtrsim 5$) and to have nonevolving mass functions with flat ($\alpha \approx -1$) low-mass slopes, are unable to reproduce the steep slope of the observed counts in this magnitude range. On the other hand, our model, which has a steep low-mass slope and much stronger evolution at low redshifts (because of many galaxies turning on star formation quite recently), reproduces the slope of the counts much better for $15 \lesssim B_J \lesssim 20$, although with our standard parameters, the predicted amplitude in this range is about a factor 2 too high, for the reason given above. The steeper slope in the counts results mainly from the steeper faint end in the LF (see Guiderdoni 1991). Figure 10 also shows the effects of varying σ_8 and f_b in the same way as in Figure 8*c*, with $f_b = (0.04, 0.09)$ for $\sigma_8 = 0.5$ and $\sigma_8 = (0.4, 0.7)$ for $f_b = 0.06$. It can be seen that the amplitude of the counts is fairly sensitive to f_b, so that a better fit to the bright counts ($B_J \lesssim 20$) would be obtained with $f_b \approx 0.04$, but at the cost of a somewhat worst fit to the bright end of the present luminosity function and to the faint counts. A better overall fit could be obtained if σ_8 were increased at the same time as f_b was reduced. Note that in phenomenological models of the luminosity function, the overall normalization of the counts (or, equivalently, the value of ϕ_* in the Schechter function fit to the present-day luminosity function) is treated as a free parameter, which most authors have adjusted to fit the observed counts at $B_J \approx 19$.

We have computed number counts in the R_F bandpass, and compared with the less extensive observational data for that band. This comparison leads to very similar conclusions to those from the B_J band data.

We show our predictions for the K-band counts in Figure 11, compared with the data from Cowie et al. (1991) and Glazebrook (1991). Our standard model is seen to fit the faint counts reasonably well, but to predict somewhat too few counts (by about a factor of 2) in the intermediate range $15 \lesssim K \lesssim 18$. The fact that our K-band counts are too low at the bright end, while our B-band counts are too high, is another manifestation of the problem that present-day galaxies

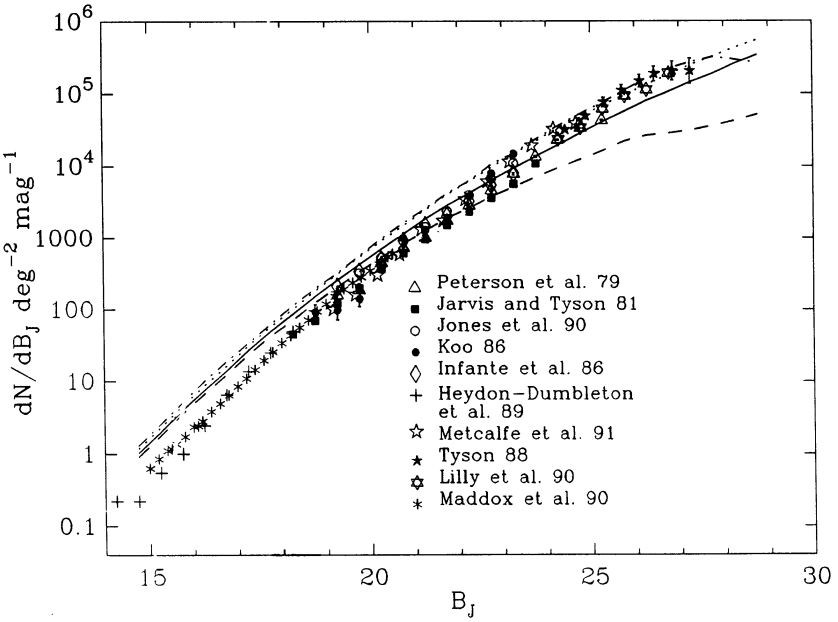

FIG. 9a

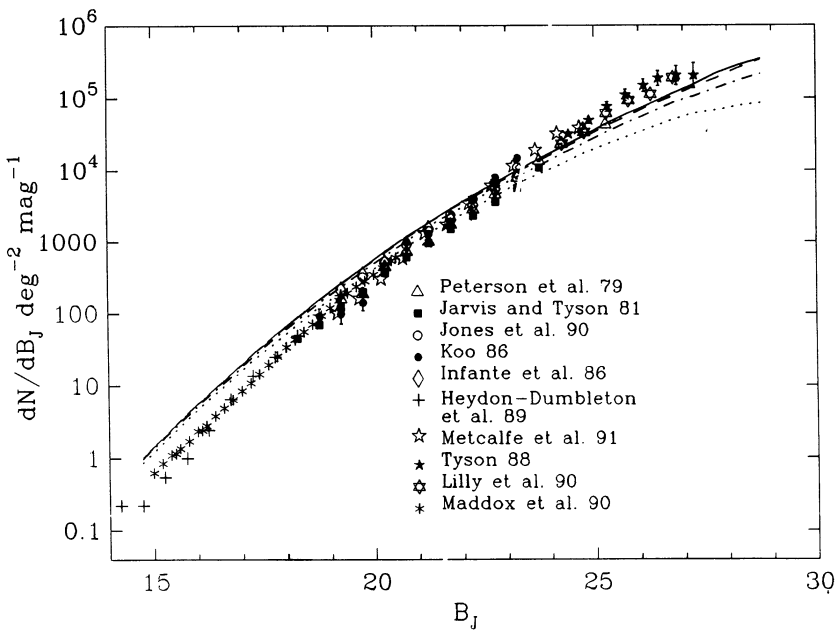

FIG. 9b

FIG. 9.—Faint galaxy counts in the B_J band. (*a*) Predicted number counts per unit isophotal magnitude, dN/dm, at a threshold $\mu_{BJ} = 28.7$ mag arcsec^{-2}, for various models of mass loss: *Dotted line*: no mass loss. *Solid* and *dot-dashed lines*: moderate mass loss, respectively with and without extra extinction. *Dashed line*: strong mass loss. Symbols show various observational determinations of counts, as follows: *Open triangles*, Peterson et al. (1979); *filled squares*, Jarvis & Tyson (1981); *open circles*, Jones et al. (1990); *filled circles*, Koo (1986); *open diamonds*, Infante, Pritchett, & Quintana (1986); *crosses*, Heydon-Dumbleton, Collins, & McGillivray (1989); *open five-pointed stars*, Metcalfe et al. (1991); *filled stars*, Tyson (1988); *open six-pointed stars*, Lilly, Cowie, & Gardner (1991); *asterisks*, Maddox et al. (1990b). The data of Tyson include his correction for incompleteness. (*b*) Predicted number counts for standard model as function of isophotal magnitudes, for various isophotal thresholds: *Solid line*: total magnitudes; *dashed*, *dot-dashed*, and *dotted lines* are for isophotal thresholds $\mu_{B_J} = (28.7, 26.55, 25)$ mag arcsec^{-2} respectively. Symbols show same observational data as in (*a*).

in our model are too blue. We emphasize again that the normalization of the counts in our model is a prediction, not a free parameter, in contrast to the work of some other authors, who treat the normalizations of the *B*-band and *K*-band counts as *independent* adjustable parameters.

4.2. *Galaxy Color Distributions*

The main observational constraints on the distribution of galaxy colors come from color distributions in apparent magnitude limited samples, since even at very low redshifts ($z < 0.1$), too few galaxies have both measured colors and measured redshifts to allow construction of useful volume-limited samples. Thus, as in the case of the number counts, the observations provide an integral constraint on the distribution of galaxies in redshift, absolute magnitude, and color, weighted toward the most luminous galaxies present at any redshift. The color distributions are sensitive to the ages of the galaxies, to details in the star-formation history such as bursts, and to

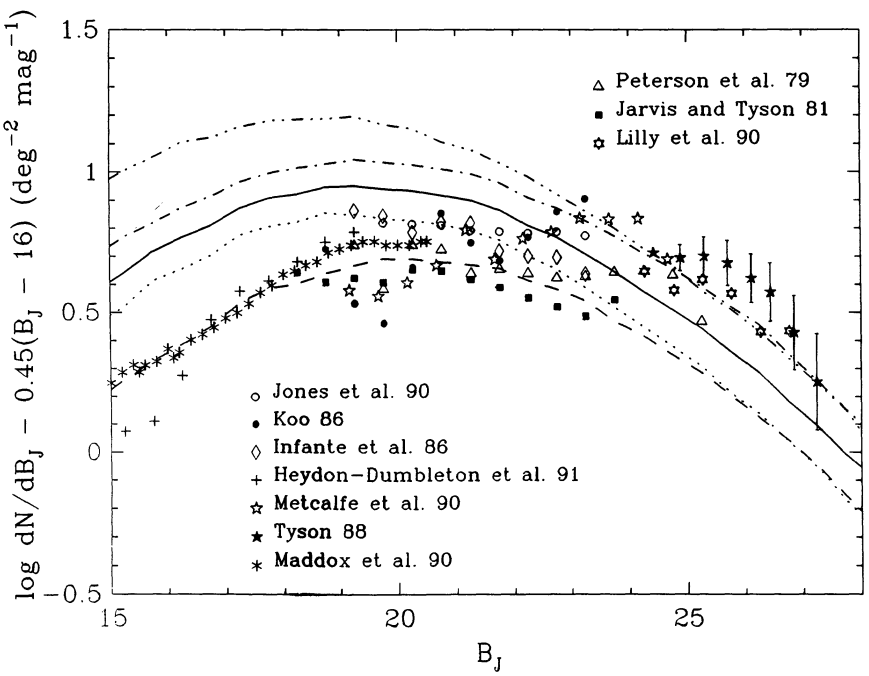

FIG. 10.—Faint galaxy counts in B_J, at an isophotal threshold $\mu_{B_J} = 28.7$ mag arcsec^{-2}, with dN/dm rescaled by dividing by a power law $10^{0.45(B_J-16)}$ mag^{-1} deg^{-2}. *Solid curve*: $\sigma_8 = 0.5, f_b = 0.06$ (our standard model). *Dashed curve*: $\sigma_8 = 0.5, f_b = 0.04$. *Dash-dot-dot-dot curve*: $\sigma_8 = 0.5, f_b = 0.09$. *Dot-dashed curve*: $\sigma_8 = 0.7$, $f_b = 0.06$. *Dotted curve*: $\sigma_8 = 0.4, f_b = 0.06$.

internal extinction. Moreover, at faint magnitudes, they may be affected by surface brightness criteria and photometric errors. So it is not surprising that these color distributions are so difficult to fit with simple scenarios for galaxy formation and evolution. Most studies, such as Yoshii & Peterson (1991) and Cowie et al. (1991), have displayed their predictions and the observations in separate plots and been satisfied with qualitative comparisons.

In Figure 12*a*, we compare predicted and observed $B_J - R_F$ distributions in an apparent magnitude limited sample with $19 < B_J < 21$. This is the brightest magnitude range for which good quality data on the color distribution have been published, yet even here, the typical galaxy redshift is $z \approx 0.2$, so that k-corrections to the colors are significant, and e-corrections cannot be neglected either. The models shown in Figure 12*a* are the same as in Figure 9*a*, while the data are taken from Jones et al. (1990), for magnitudes corrected to "total." In all of the plots of Figure 12, the predicted distributions have been normalized to the same area as the observational histograms and convolved with Gaussians to represent the effects of observational errors, with dispersions $\sigma = 0.10$ for Jones et al. and $\sigma = 0.15$ for Metcalfe et al. (1991). This does not have a significant effect on the number counts and so has not been included in those plots. The predicted color distribution is fairly insensitive to the assumptions about mass loss, but somewhat more sensitive to the model for extinction. The model without additional extinction is too blue, due to the presence in the luminosity function of many bright galaxies with very blue colors. Including the extra $\Delta A_V = 1$ mag extinction on massive (OB) stars results in a good fit to the observations.

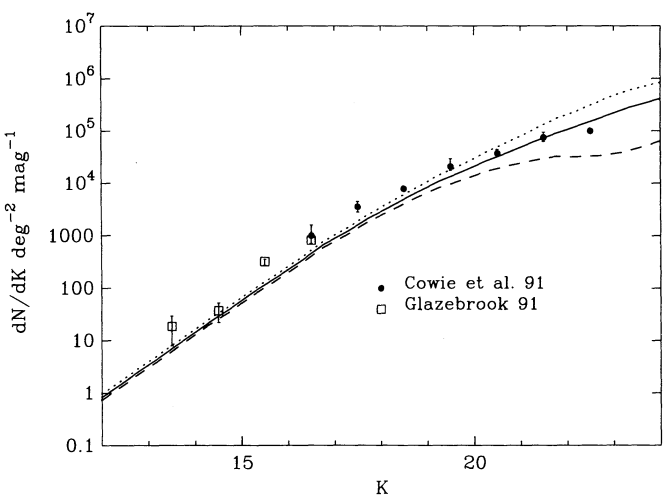

FIG. 11.—Faint galaxy counts in the K band. *Dotted*, *solid*, and *dashed curves* are the models with no, moderate, and strong mass loss respectively. Solid curve is our standard model. Symbols show observational data from Cowie et al. (1991) and Glazebrook et al. (1991).

Figures 12*b*–12*d* show how the $B_J - R_F$ color distribution changes as one goes to fainter apparent magnitudes. The models are the same as in Figure 12*a*, and are compared with the data from Metcalfe et al. (1991), for $B_J = 22$–24. The median redshift increases, to $z \approx 0.35$ for $B_J \approx 24$, so that the visible bandpass more and more probes the rest-frame UV. The models get slightly redder with increasing magnitude, while the observed distributions get gradually bluer. Our standard model is significantly too red compared to observations for $B_J \gtrsim 23$. This might suggest that the internal extinction decreases with increasing look-back time more rapidly than assumed in our models (which allow for evolution in the uniform component of extinction, but not in the additional extinction on OB stars). Predictions for the color distributions at fainter magnitudes will be presented in § 5.2. The observational data at these magnitudes are still rather uncertain.

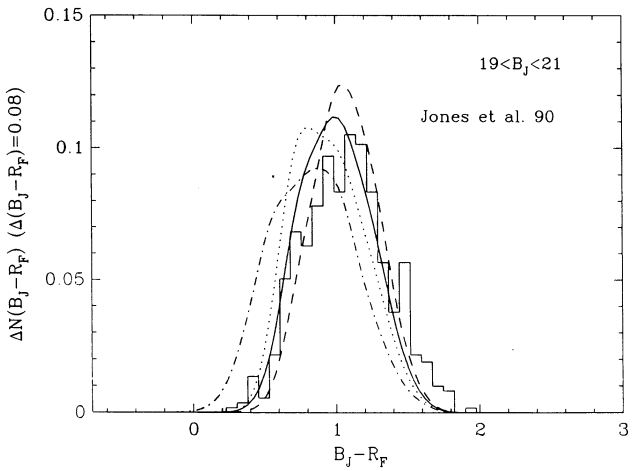

FIG. 12*a*

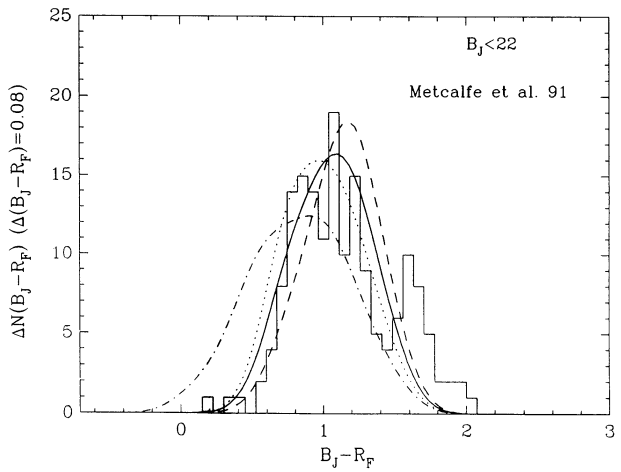

FIG. 12*b*

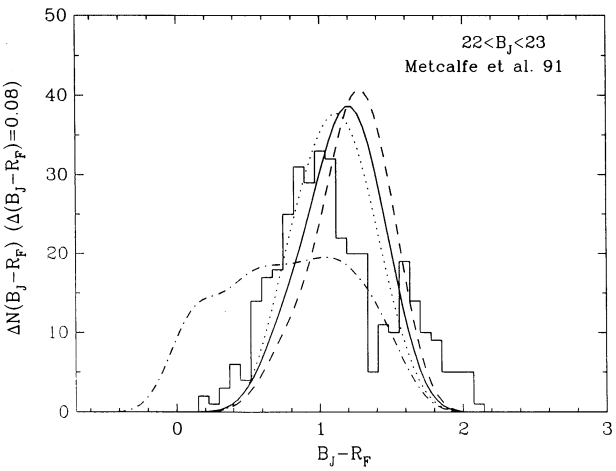

FIG. 12*c*

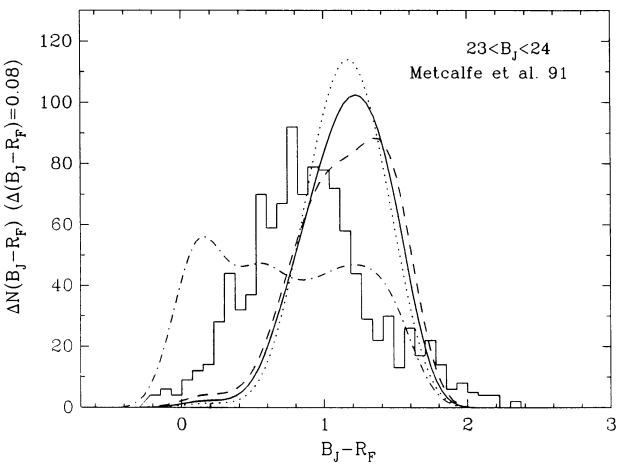

FIG. 12*d*

FIG. 12.—$B_J - R_F$ color distributions in apparent magnitude limited samples. Curves show model predictions: *Dotted*, *solid*, and *dashed lines*: no, moderate and strong mass loss respectively, with extra extinction. *Dot-dashed*: moderate mass loss, without extra extinction. Histograms shows observational data. The models have been convolved with Gaussians of dispersion σ to represent the effects of observational errors, and normalized to the same area as the observational histograms. (*a*) Predictions for $19 < B_J < 21$ compared to observations from Jones et al. (1990) (with $\sigma = 0.10$), plotted as number fractions per bin. (*b*), (*c*), and (*d*) Predictions for $B_J < 22$, $22 < B_J < 23$, and $23 < B_J < 24$, respectively, compared with observational data from Metcalfe et al. (1991) (with $\sigma = 0.15$), plotted as number per bin.

4.3. *Redshift Distributions*

More detailed information about the evolution of the galaxy luminosity function can be obtained by measuring the redshift distributions in various apparent magnitude-limited samples. In principle, by measuring the distribution of galaxies in m and z for a set of different bandpasses, one could reconstruct empirically the entire past evolution of the galaxy luminosity function. In practice, current observational data are too limited for this, but the measured redshift distributions still provide vital constraints on the models.

The predicted redshift distributions are obtained by integrating equation (13) over the relevant range of apparent magnitude. Figure 13 shows comparisons between predicted and observed redshift distributions for galaxy samples in the magnitude range $20 < B_J < 24$. In Figures 13*a*–13*b* we compare respectively with data from Broadhurst, Ellis, & Shanks (1988) for $20 < B_J < 21.5$ (187 redshifts), and Colless et al. (1990) for $21 < B_J < 22.5$ (87 redshifts). In both cases, predicted distributions have been normalized to the same total number of redshifts as the observations. The magnitudes are isophotal, but the model results are little different if one uses total magnitudes instead. Note that the error bars on the data do not include the effects of galaxy clustering and so somewhat underestimate the true uncertainties (for instance, Broadhurst et al. mention a cluster in their sample at $z \approx 0.15$–0.20). In general, our standard model agrees well with the observations, in particular in the lack of a large high-redshift tail. The main discrepancy is the excess of low redshift ($z \lesssim 0.1$) objects predicted by the models, which is particularly apparent in the Broadhurst et al. sample, where the excess is a factor of ~ 4 for $z < 0.1$. This excess results from the large number density of nearby dwarf galaxies in the model, due to the steep faint-end slope of the present luminosity function. These dwarfs are the faded relics of the galaxies which at higher redshifts are responsible for the faint ($B \gtrsim 24$) counts. The constraint on the faint-end slope of the present luminosity function from their data was already emphasized by Broadhurst et al. This disagreement between models and data could be a result of incompleteness in the

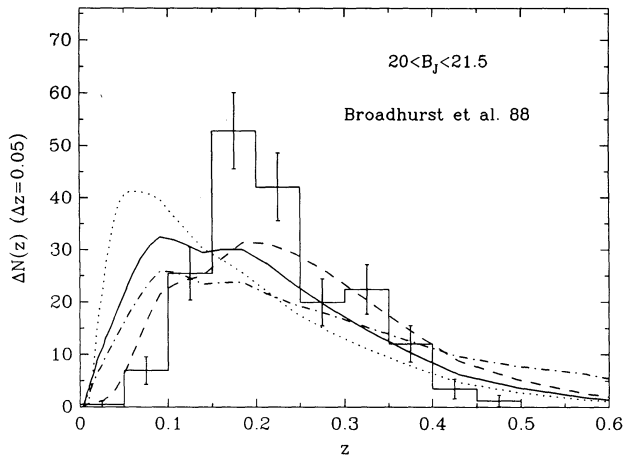

FIG. 13*a*

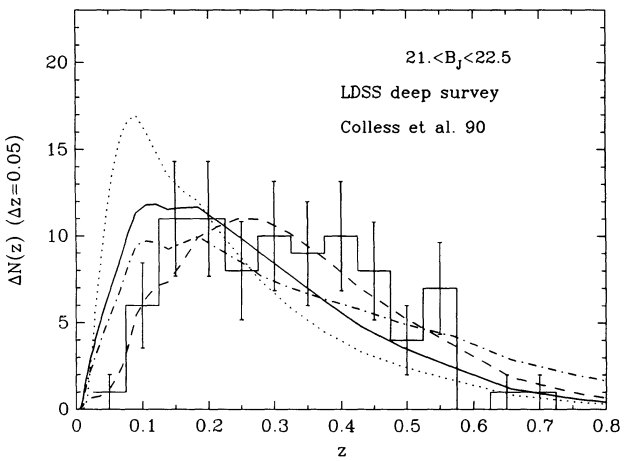

FIG. 13*b*

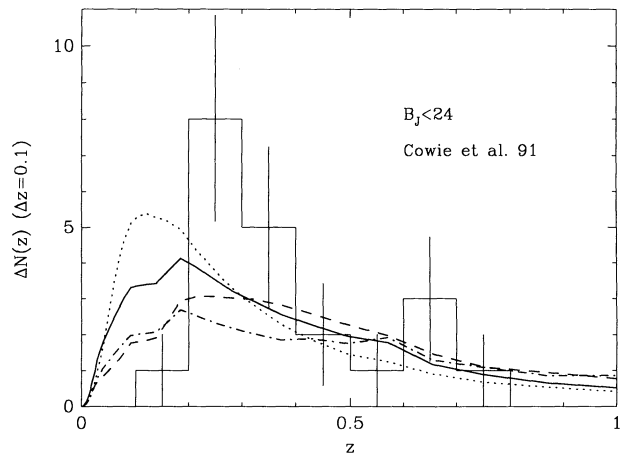

FIG. 13*c*

FIG. 13.—Redshift distributions for apparent magnitude limited samples. Curves show models: *dotted*, *solid*, and *dashed curves* are for no, moderate, and strong mass loss, respectively. *Dot-dashed curve* shows moderate loss model without extra extinction. Histograms and points with Poisson error bars show observational data, plotted as number per bin. (*a*) For $20 < B_J < 21.5$, compared with observational data from Broadhurst et al. (1988) (isophotal magnitudes with threshold $\mu_{B_J} = 26$ mag arcsec^{-2}). (*b*) For $21 < B_J < 22.5$, compared with data from Colless et al. (1990) (isophotal magnitudes with threshold $\mu_{B_J} = 26.55$ mag arcsec^{-2}). (*c*) For $B_J < 24$, compared with data from Cowie et al. (1991) (total magnitudes).

observational sample. The Broadhurst et al. sample is only 85% complete, so the discrepancy would be removed if the unidentified 15% of objects were all galaxies with $z < 0.1$. There might be a bias against measuring redshifts for these nearby dwarfs because of their lower surface brightnesses, or because they lack [O II] emission lines (because most of them are no longer forming stars), or because they have weak Ca H and K lines (because they have low metallicity). Broadhurst et al. excluded objects from their sample on the basis of "stellar" morphology, and some of these objects might be dwarfs, but Colless et al. separated stars from galaxies spectroscopically, and obtained similar results, suggesting that this is not a major problem.

In Figure 13*c* we compare with the observed redshift distribution from Cowie et al. (1991) for $B_J < 24$, which consists of 21 measured redshifts out of a sample of 22 galaxies. The model curves are normalized to the same number of redshifts as are observed. This is the deepest field galaxy redshift survey yet published. Again, our standard model is in reasonable agreement with the data. As we discuss further in § 5.2, at these magnitudes, the galaxy distribution in our model is becoming dominated by dwarf galaxies, in agreement with the conclusion reached by Cowie et al. from their data.

5. FURTHER PREDICTIONS OF THE MODEL

In this section we present some further predictions of the models, divided into (*a*) integrated quantities, (*b*) specific predictions for the properties of galaxies seen in the faint counts ($B > 24$), which we hope may be soon become testable, and (*c*) properties of non–star-forming "dark" galaxies.

5.1. *Integrated Quantities*

Figure 14 shows the star formation rate per unit comoving volume as a function of redshift, integrated over all masses, and also separately for the mass ranges $M_b < 10^9\ M_\odot$, $10^9 < M_b < 10^{11}\ M_\odot$, and $M_b > 10^{11}\ M_\odot$. It can be seen that the total star formation rate peaks at $z \approx 1.5$, but then declines by only a factor of 2.5 up to the present day, with a current total star formation rate per unit volume of $2.5 \times 10^7\ M_\odot\ \mathrm{Gyr}^{-1}$

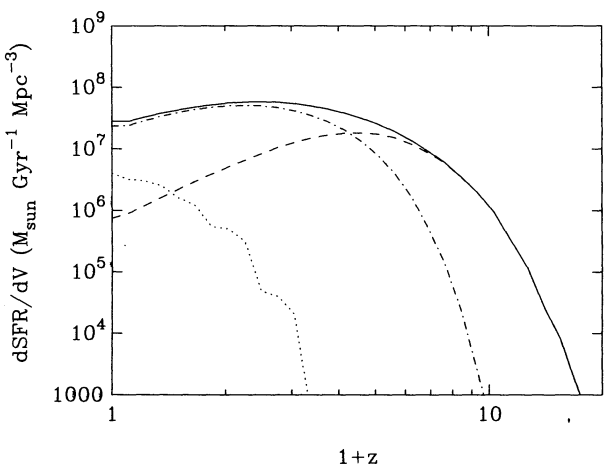

FIG. 14.—Predicted star formation rate per unit comoving volume, as a function of redshift. *Solid curve*: star formation rate integrated over all masses. *Dashed*, *dash-dot*, and *dotted curves* are star formation rates for the mass ranges $M_b < 10^9\ M_\odot$, $10^9 < M_b < 10^{11}\ M_\odot$, and $M_b > 10^{11}\ M_\odot$, respectively.

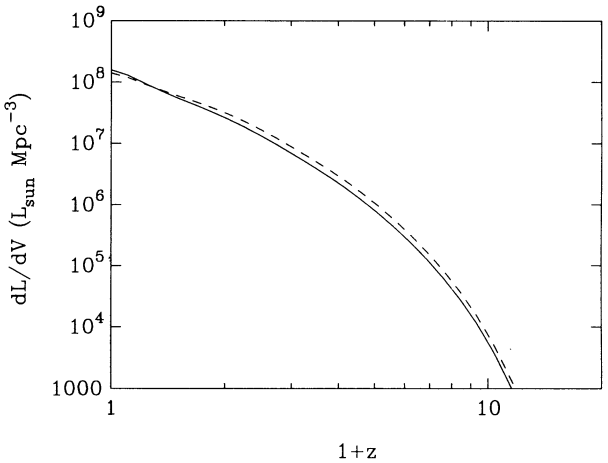

FIG. 15.—Rest-frame luminosity densities, per unit comoving volume, integrated over all galaxies in the *B*-band (*solid curve*) and the *R*-band (*dashed curve*), vs. *z*.

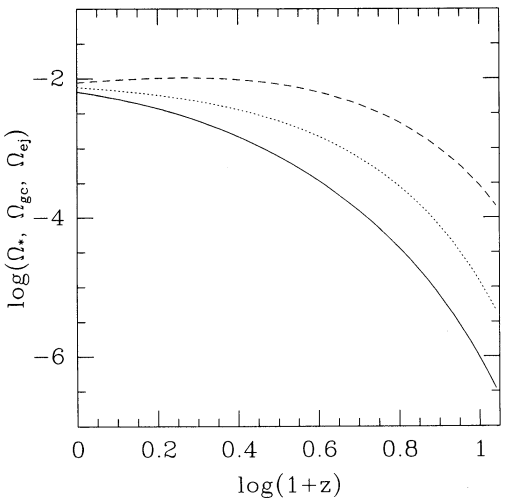

FIG. 16.—Fractions of critical density in form of stars (*solid curve*), cold gas (*dashed curve*), and ejected gas (*dotted curve*), as functions of redshift.

Mpc^{-3}. Half of the stars currently existing form at $z < 0.7$. As expected, the net star formation rate in lower mass galaxies peaks at higher redshifts. Figure 15 shows how the comoving luminosity densities in the *B* and *R* bands vary with redshift. These both increase steadily up to the present day, with a predicted present luminosity density $\mathscr{L}_B = 1.5 \times 10^8 L_{B\odot}$ Mpc^{-3} in the *B* band. This compares with a value $\mathscr{L}_B = 7 \times 10^7 L_{B\odot}$ Mpc^{-3} found by integrating over Loveday et al.'s (1991) Schechter function fit to the observed luminosity function, extrapolated down to low luminosities. The reason for the discrepancy is, of course, the excessive number of fainter ($L < L_*$) galaxies in our predicted luminosity function. Figure 16 shows, as a function of redshift, the fraction of the critical density in the form of stars, Ω_* (including the effects of mass loss), cool ($T < 10^4$ K) gas in galaxies, Ω_{gc} (whether star forming or not), and in gas which has been ejected from dwarf galaxies by supernova-driven winds, Ω_{ej}. Some of this ejected material may end up later in the form of cool gas or stars, but this effect has not been included. The present values of these fractions are $\Omega_* = 6 \times 10^{-3}$, $\Omega_{gc} = 9 \times 10^{-3}$, and $\Omega_{ej} = 8 \times 10^{-3}$, out of a total baryonic fraction $\Omega_b = 0.06$. The remainder of the baryons are in gas at the virial temperature in galaxy halos. Figure 17 shows the rest-frame luminosity functions in the *U*, *B*, *R*, and *K* bands, for redshifts $z = (0, 2, 4, 6)$. In all these bands, there is an increase in the number of galaxies

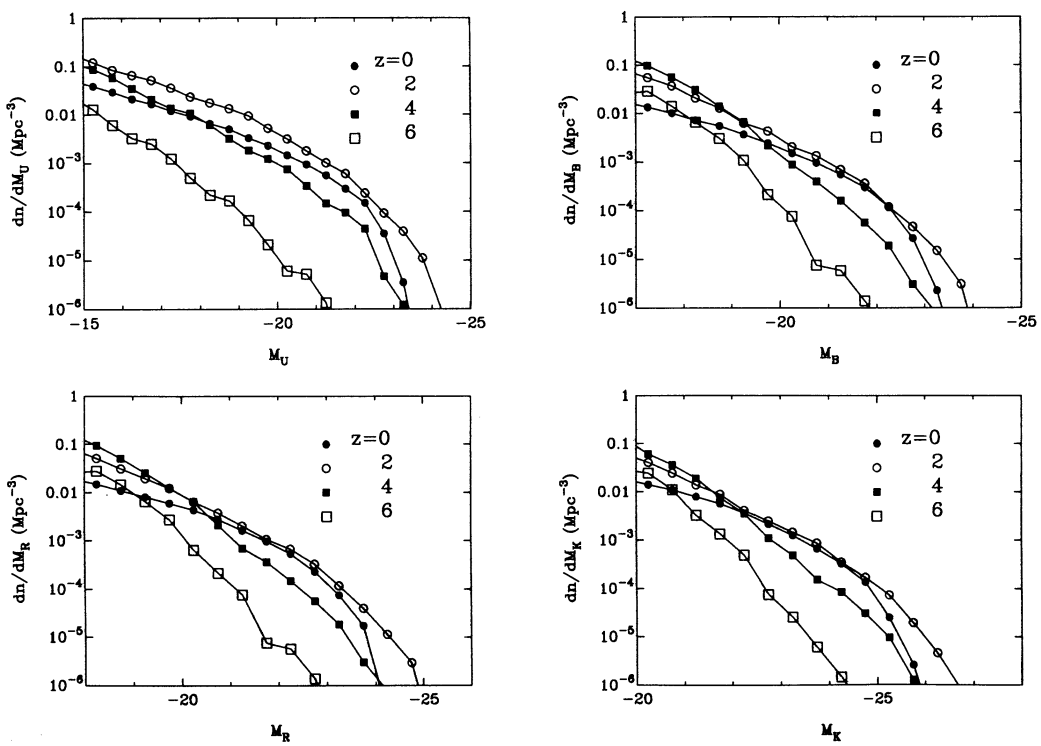

FIG. 17.—Rest frame luminosity functions in *U*, *B*, *R*, and *K* bands, at redshifts $z = (0, 2, 4, 6)$

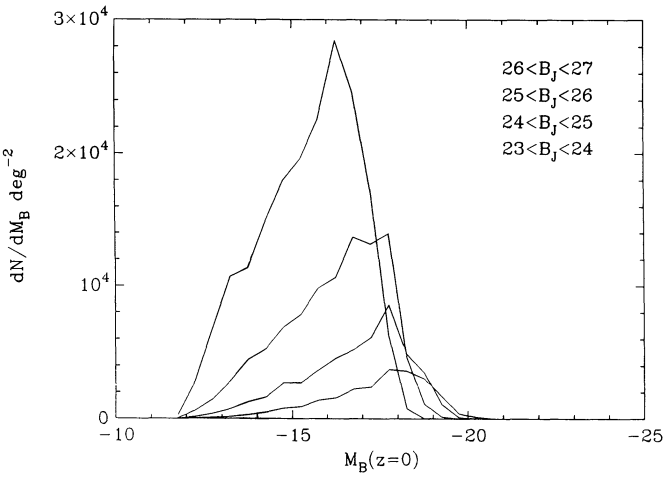

FIG. 18.—Predicted distributions of current absolute magnitude for galaxies seen at various apparent magnitudes. The number of objects per unit absolute magnitude $\mathcal{M}_B(z = 0)$ per unit solid angle are given for the apparent magnitude ranges $24 < B_J < 25$, $25 < B_J < 26$ and $26 < B_J < 27$, with the higher curves corresponding to fainter magnitudes.

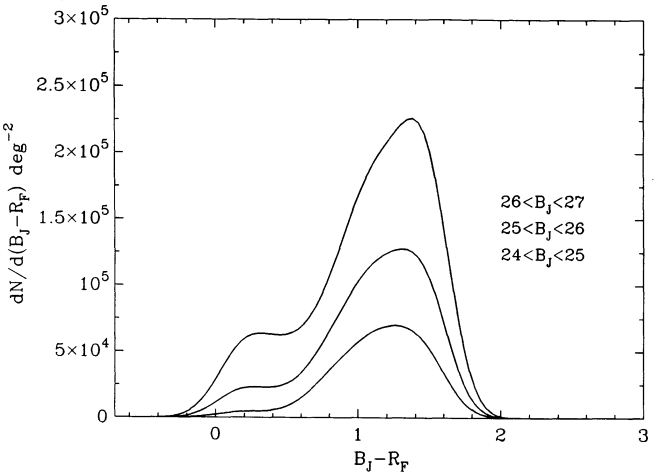

FIG. 20.—Predicted $B_J - R_F$ color distributions for faint galaxies. The number of objects per unit color per unit solid angle are given for the same magnitude ranges as in Fig. 19, with the higher curves corresponding to fainter magnitudes. The curves have been smoothed with a Gaussian of dispersion $\sigma = 0.15$.

at both the bright and faint ends of the ranges plotted for $z \lesssim 2$, due to evolutionary brightening (which more than compensates for the loss of some objects from the high end of the mass function). For $z \gtrsim 2$, one starts to lose objects from the bright end of the luminosity function due to the effect of galaxies not yet having turned on star formation, and this depletes the low-luminosity end also for $z \gtrsim 4$. These results can be compared with those predicted by the phenomenological number density evolution model of Rocca-Volmerange & Guiderdoni (1990) and Guiderdoni & Rocca-Volmerange (1991), in which the galaxy mass function is assumed to evolve, always keeping the Schechter function form, and conserving the total mass. They found that to fit the same observational data as compared within this paper, they needed evolution in the sense of having fewer massive and more dwarf galaxies at high redshift.

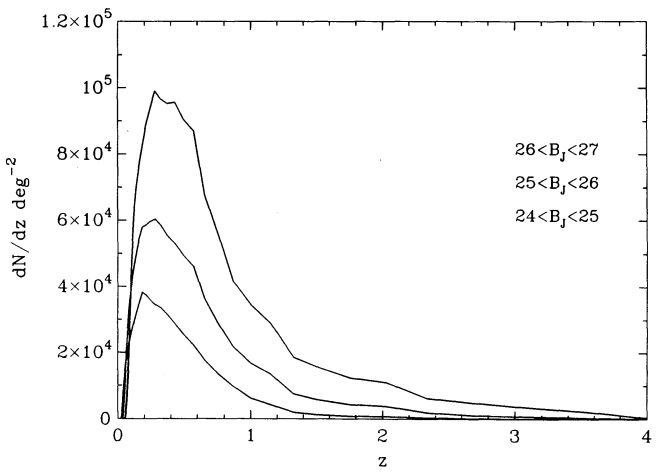

FIG. 19.—Predicted redshift distributions for faint galaxies. The number of objects per unit redshift per unit solid angle are given for $24 < B_J < 25$, $25 < B_J < 26$ and $26 < B_J < 27$ respectively, with the higher curves corresponding to fainter magnitudes.

5.2. *Predicted Properties of Faint Galaxies*

Here we present some predictions for the properties of the galaxies seen in the faint counts at $B > 24$, which we hope will become directly testable in the near future.

Figure 18 shows the distributions of *present* luminosities for galaxies seen in the faint counts at various apparent magnitudes in the range $B_J = 23$–27. It can be seen that at $B_J \approx 24$, the counts are already dominated by galaxies with quite low present luminosities, $\mathcal{M}_B \sim -18$, and going to fainter magnitudes, the typical present luminosity shifts to even lower values, reaching $\mathcal{M}_B \sim -15$ for $B_J \approx 27$. Thus in our model, the number counts at faint magnitudes ($24 < B_J < 27$) are dominated by dwarfs, which mostly begin forming stars at redshifts $0.5 \lesssim z_* \lesssim 2$, and form stars on time scales $0.1 \lesssim \tau_* \lesssim 1$ Gyr, with somewhat larger z_* and shorter τ_* for the fainter objects.

In Figure 19, we show predicted redshift distributions for magnitude-limited samples in the range $B_J = 24$–27. Median redshifts for $B_J = 20$–27 are given in Table 1. The median redshift increases only slowly with increasing magnitude, reaching $z \approx 0.4$ at $B_J = 23$–24 and $z \approx 0.6$ at $B_J = 26$–27. Even at $B_J = 27$, the fraction of objects with $z > 2$ is predicted to be very small.

Figure 20 shows the predicted $B_J - R_F$ color distributions for

TABLE 1

MEDIAN AND QUARTILE REDSHIFTS AND COLORS FOR STANDARD MODEL

B_J	$z_{1/4}$[a]	$z_{1/2}$[b]	$z_{3/4}$[c]	$(B-R)_{1/4}$[a]	$(B-R)_{1/2}$[b]	$(B-R)_{3/4}$[c]
20–21.....	0.10	0.17	0.26	0.8	1.0	1.2
21–22.....	0.12	0.21	0.33	0.9	1.1	1.2
22–23.....	0.15	0.27	0.42	0.9	1.1	1.3
23–24.....	0.19	0.31	0.50	0.9	1.1	1.3
24–25.....	0.22	0.39	0.62	0.9	1.1	1.3
25–26.....	0.27	0.48	0.81	0.8	1.1	1.4
26–27.....	0.33	0.57	1.02	0.8	1.1	1.4

[a] Lower quartile.
[b] Median.
[c] Upper quartile.

the same magnitude ranges. Median colors are given in Table 1, and are quite red, $B_J - R_F \approx 1.1$ throughout the range $B_J =$ 21–27. (For comparison, note that a "flat spectrum" source, with $f_\nu =$ constant, would have $B_J - R_F = 0.16$.) The reason for the red colors at faint magnitudes is that the dwarfs which then dominate the counts are seen *after* their initial burst of star formation has been terminated by mass loss.

Figure 21 shows predicted angular diameters for the faint galaxies, both at the half-light isophote, and at an isophote $\mu_{BJ} = 28.7$ mag arcsec^{-2}. The fainter objects are predicted to have smaller angular sizes. Tyson (1988) reports that galaxies with $26 \lesssim B_J \lesssim 27$ have half-light diameters $\theta_e \approx 0''.8$, somewhat larger than the prediction of our model, but Tyson's galaxy images are dominated by seeing effects, so his derived "true" sizes are rather uncertain.

5.3. *Properties of Non–Star-forming Galaxies*

An important prediction of our model is that there should be halos in which the gas has cooled, but in which star formation has not yet begun because the surrounding galaxy group has not yet collapsed. Figure 22 shows the cumulative distribution of hydrogen masses, $n(>M_H)$ versus M_H, for the cool gas both in "dark galaxies" and in luminous, star-forming galaxies. (The mass fraction of hydrogen in the gas is assumed to be 76%.) It can be seen that most ($\sim$90%) of the cool gas is in the "dark" galaxies, although the present total mass fractions in the two types of galaxy (including stars in the luminous galaxies) are comparable: Ω_b(luminous galaxies) = 0.007 and Ω_b(dark galaxies) = 0.008, respectively.

If the cool gas in the dark galaxies is in the form of atomic hydrogen (H I), it should emit radiation in the 21 cm line. Observational searches have been conducted for 21 cm emission from isolated intergalactic clouds containing H I but having no optical emission, with essentially negative results. The limits set by two of these searches, by Fisher & Tully (1981) and by Briggs (1990), are shown in the figure. These limits are expressed in the form $n(>M_H) < 3/V(M_H)$, where $V(M_H)$ is the volume of space within which the search would detect objects of mass M_H, and the factor of 3 gives a 95% confidence upper limit on the true density if the number of objects detected is zero. It is important to note that these limits assume that (1) the angular size of the objects is smaller than the beam of the radio telescope used; (2) the hydrogen is optically thin in the 21 cm line; and (3) the hydrogen has spin temperature $T_S \gg 3$ K, the temperature of the microwave background. If any of these conditions are violated, then the limits are weakened. In addition, the derived limits depend on the width Δv of the integrated 21 cm velocity profile of the objects. Fisher & Tully assumed $\Delta v < 100$ km s^{-1}, while Briggs does not state the value he used. The limits on the number density weaken in proportion to $(\Delta v)^{3/2}$, which could be a significant effect for higher masses, given that $\Delta v \approx 2V_c$. In any case, Briggs' limits lie as much as a factor of 100 below our prediction for "dark" galaxies, so that either the model is wrong, or one of the assumptions made in deriving the 21 cm upper limits is incorrect. Assumption (1) is probably safe, given the galaxy sizes predicted by our model, but assumption (2) may be violated. As discussed below, the typical column density for the dark galaxies is expected to be $N_H \sim 10^{22}$ cm^{-2}, so if the gas is very cool, $T \lesssim 100$ K, and in a thin layer with a low velocity dispersion $\sigma \lesssim 10$ km s^{-1}, the 21 cm optical depth would be quite large, $\tau \gtrsim 10$, which would greatly suppress the 21 cm emission, and weaken the limits in proportion to $\tau^{3/2}$, bringing them more into line with the model. Alternatively, it is possible that most of the hydrogen is ionized, as is the case for Lyα-forest clouds, or in molecular form.

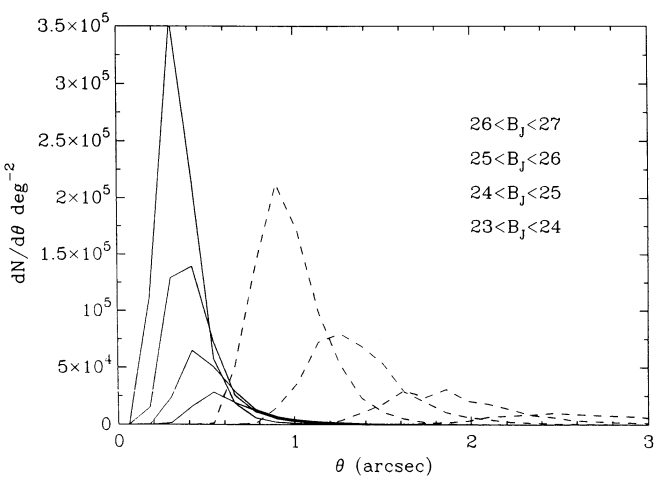

FIG. 21.—Predicted angular diameter distributions for faint galaxies. The number of objects per unit diameter θ per unit solid angle are given for the same magnitude ranges as in Fig. 18, with the higher curves corresponding to fainter magnitudes. *Solid curves*: half-light diameters. *Dashed curves*: isophotal diameters at $\mu_{BJ} = 28.7$ mag arcsec^{-2}. These sizes do not include the effects of seeing.

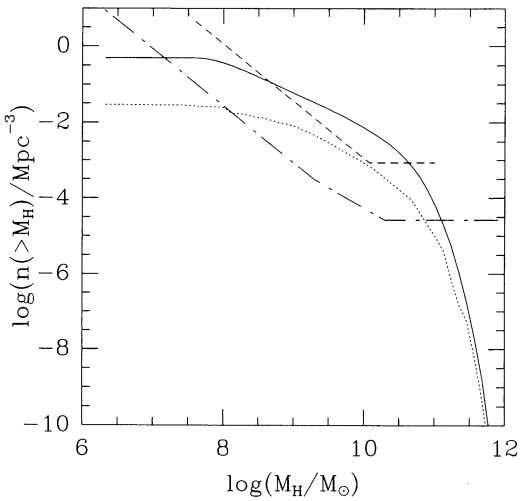

FIG. 22.—Present cumulative mass function for cold hydrogen gas. $n(>M_H)$ is the number density of galaxies with hydrogen masses larger than M_H. *Solid curve*: predicted distribution for galaxies which have not yet begun star formation ("dark galaxies"). *Dotted curve*: predicted distribution for luminous, star-forming galaxies. Also shown are observational upper limits from 21 cm emission, from Fisher & Tully (1981); *dashed curve*, and Briggs (1990); *dot-dashed curve*, plotted as explained in the text.

An alternative method of detecting atomic hydrogen in dark galaxies is to look for absorption against bright background sources, either 21 cm absorption against radio galaxies or Lyα absorption against quasars. In this case, a large 21 cm optical depth would be favorable to detection. In Figure 23, we show the predicted number of absorption features per unit redshift per logarithmic interval in N_H, at $z = 0$, for the case that all the cool hydrogen is in the form of H I. This is calculated in the following way: for each dark or luminous galaxy, the gas is assumed to be in a uniform surface density disk, with half-mass radius r_* given by the model, as explained in § 2.2. We then

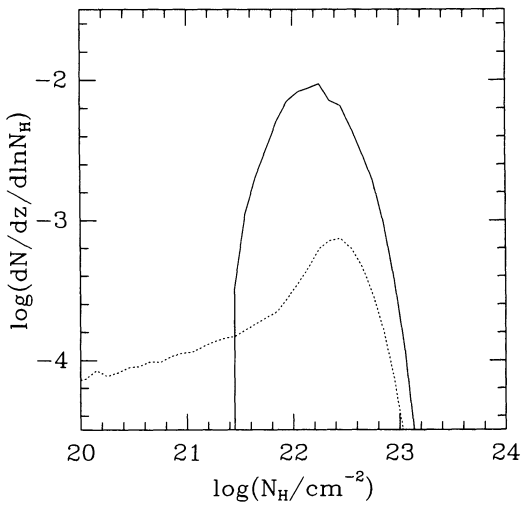

FIG. 23.—Predicted frequency of hydrogen absorption features, per unit redshift, per unit log hydrogen column density. Solid and dotted lines show contributions from dark and luminous galaxies, respectively.

assign each galaxy an absorption cross section $A_H = \pi r_*^2$ and column density $N_H = M_H/(m_H A_H)$, where m_H is the mass of a hydrogen atom, and a factor of $\frac{1}{2}$ has been included in the formula for A_H to account for the fact that a disk will on average be inclined at 60° to the line of sight. The predicted distribution of absorptions is seen to be dominated by the dark galaxies and to have a rather narrow distribution in column densities around $N_H \sim 2 \times 10^{22}$ cm^{-2}. This reflects the fact that r_* (before the effects of mass loss) nearly follows the constant surface density relation $r_* \propto M_b^{1/2}$ over the mass range $10^8 \lesssim M_b \lesssim 10^{11}\ M_\odot$. This is shown in Figure 5*a* for star-forming galaxies, but dark galaxies follow a similar relation, except with radii r_* that are typically a factor of 2 larger at a given mass. The total probability for absorption with $N_H > 10^{21}$ cm is $dN/dz = 1.8 \times 10^{-2}$. (Our calculation of the column density distribution is rather simplified. The effects of allowing for a nonuniform surface density profile and a distribution of inclinations are discussed by Milgrom (1988). For a smooth, monotonically declining surface density profile, the main effect is to extend the distribution down to lower values of N_H, but the result depends entirely on the assumed form for the profile, so we have not made any more detailed calculation.) In a search for 21 cm absorption against radio sources with $0 < z < 1$, Brown (1988) finds a frequency of absorption $dN/dz \gtrsim 2 \times 10^{-2}$ for $N_H \gtrsim 10^{21}$ cm$^{-2}(T_S/300$ K), which seems compatible with what our model predicts at $z \approx 0$. At higher redshifts, $z \gtrsim 1.5$, H I in the dark galaxies will contribute to the Lyα absorption lines seen at optical wavelengths in the spectra of quasars. Turnshek et al. (1989) find that the mean frequency of damped Lyα absorption lines with $N_H > 2 \times 10^{20}$ cm^{-2} in the interval $1.8 < z < 2.6$ is $dN/dz \approx 0.3$. This is larger than the prediction of our model with uniform disks, for which $dN/dz \approx 0.02$ for $N_H > 2 \times 10^{20}$ cm^{-2} and $0 \lesssim z \lesssim 2$ and falls off at higher redshifts. Thus, to explain the large observed frequency of damped Lyα systems, we would need to consider disks with nonuniform surface density profiles. Note that at any redshift, the total H absorption cross section at high column densities is predicted to be dominated by galaxies not yet undergoing star formation.

6. DISCUSSION AND CONCLUSIONS

We have presented a model for the evolution of the galaxy luminosity function, in which the distribution of galaxy masses, star formation time scales, and star formation turn-on redshifts is derived from the initial power spectrum of density fluctuations, under the assumption that galaxies form at peaks of the initial density field, and that the star formation rate is controlled by the frequency of interactions with neighboring galaxies. We have assumed that the power spectrum is that predicted by CDM, but our model is only sensitive to the form of the spectrum on galaxy scales, not to its large-scale behavior. Star formation occurs within the baryonic cores formed by condensation within dark halos satisfying a cooling condition, and the baryons are assumed to collapse by a constant factor in radius compared to the parent halo. We assume that there is no merging of the luminous components of galaxies. Galaxies having low escape velocities are assumed to lose most of their gas via supernova-driven winds, reducing the efficiency of star formation by a factor proportional to the square of the halo circular velocity. The luminosities and colors of the stellar components of galaxies are calculated using a population synthesis model.

The most important features of the model are (1) The mass function of galaxy halos is very steep at low masses, $dn/dM \propto M^{-2}$. This is a robust prediction of CDM and is obtained whether one calculates the mass function using N-body simulations, or the Press-Schechter method, or, as here, the peaks formalism. This steep mass function translates into a steep luminosity function, unless the effects of mass loss are very strong. On the one hand, this provides plenty of objects to explain the faint galaxy counts, but on the other hand, it also predicts a steep slope for the present-day luminosity function, which appears to be in conflict with the observed field luminosity function, to the extent that this is complete for low-luminosity, low surface brightness galaxies. (2) Star formation occurs quite late, especially for massive galaxies, because it is assumed to begin only when the group surrounding a galaxy has collapsed, and tidal encounters commenced. This leads to a serious failing of our model, namely, that the brightest objects in the present luminosity function are predicted to be very blue, with too few objects having the red colors and old stellar populations of elliptical galaxies. On the other hand, the late epoch of star formation helps in producing a steep slope for the number counts at bright magnitudes, in better agreement with observations than more standard models, although the main factor here is the steep slope of the present LF.

We can summarize the success of the model as follows:

1. We find a quite good fit to the present luminosity function for bright galaxies ($\mathcal{M}_B \lesssim -20$). The bright-end cutoff in the model results from our cooling condition, while the number density at the "knee" of the luminosity function turns out correctly because of our group collapse condition for star formation to begin, which results in a type of "biasing" of the luminous galaxies relative to the mass.

2. We obtain a good fit to the relation between half-light radius and luminosity for galaxies fainter than $\mathcal{M}_B \gtrsim -21$. For galaxies brighter than this, the predicted radii are too small compared to those observed.

3. The relation we predict between halo circular velocity and blue luminosity for bluer ($B-V < 0.8$) galaxies is consistent with the observed Tully-Fisher relation for spiral galaxies. In particular, if we separate galaxies by color, we find $L_B \propto V_c^4$,

in good agreement with the Tully-Fisher slope found for individual morphological types. For the redder ($B-V > 0.8$) galaxies, the predicted relation between blue luminosity and central velocity dispersion seems approximately consistent with the observed Faber-Jackson and "fundamental plane" relations for elliptical galaxies, if we assume that the halo circular velocity is related to the observed stellar velocity dispersion by $V_c = (3)^{1/2}\sigma_*$, but the observational and theoretical justifications for the latter assumption are rather weak, so this should not be considered a strong result.

4. We find a reasonable fit to the B- and R-band number counts up to $B \lesssim 24$ whatever mass-loss model we assume, as these counts are predicted to be dominated by fairly massive galaxies. In particular, we find a good fit to the slope seen in the bright counts ($15 \lesssim B \lesssim 20$), although the predicted amplitude there is somewhat too high, due to the factor 2 excess in the number of galaxies at $\mathcal{M}_B \approx -20$ in our local LF. On the other hand, for the faintest counts ($B \gtrsim 24$), our predictions are sensitive to how effective we assume mass loss to be. We only reproduce the observed counts at these magnitudes if the mass loss is not too strong. In that case, we predict that the faint counts at $24 \lesssim B \lesssim 27$ should be dominated by dwarf galaxies, with $M_b \sim 10^9$–10^{10} $M_\odot$, $V_c \sim 50$–100 km s^{-1}, at redshifts $z \sim 0.2$–1. These galaxies would have begun star formation at $z_* \sim 0.5$–2, and formed stars on a time scale $\tau_* \sim 0.1$–1 Gyr, before having their remaining gas ejected by a wind. They are seen in the counts mostly after their initial burst phase. They should have apparent angular diameters $\theta_e \sim 0''.2$–$1''$. By now they would have faded to objects with absolute magnitudes $-18 \lesssim \mathcal{M}_B \lesssim -14$. We have also computed counts in the K band. For our standard model, these agree well with the observations at faint magnitudes, but are somewhat low at the bright end, $K \lesssim 18$.

5. We reproduce the observed $B-R$ color distributions seen in apparent magnitude limited samples at $10 \lesssim B \lesssim 23$, when we include both the standard $A_V \sim 0.3$ mag extinction applied to all stars and an extra $\Delta A_V = 1$ mag extinction on massive (OB) stars only. The extra extinction is needed to counteract the effect of the very blue colors of the most luminous galaxies in the model. At fainter magnitudes, our predicted colors start to become too red.

6. Our predicted redshift distributions in apparent magnitude-limited samples are in reasonable accord with the observational data at $20 \lesssim B \lesssim 24$. In particular, our model does not give an excessive number of high-redshift galaxies. We do, however, predict an excess of galaxies at low redshifts, $z \lesssim 0.1$, compared to the observations, due to the same dwarf galaxy population which at higher redshifts is responsible for the faint counts in our model.

The main problems are

7. Our standard model predicts a present luminosity function with a fairly steep faint-end slope, $dn/dL \propto L^{-1.6}$ (i.e., $\alpha \approx -1.6$). While the observed luminosity functions in some clusters are nearly this steep, the field luminosity function appears to be much flatter, $\alpha \approx -1$, at least for galaxies with $\mathcal{M}_B \lesssim -17$ and surface brightnesses $\langle \mu_B \rangle_e \lesssim 24$ mag arcsec^{-2}. We could produce a flatter luminosity function if we assumed much stronger mass loss, but this would result in the predicted faint ($B \gtrsim 24$) counts being too low. An alternative possibility is that most of the low-luminosity galaxies have such low surface brightnesses that they are missing from the observational samples. However, for the surface brightnesses predicted by our model, based on a uniform collapse factor $f_{\rm diss}$ for all galaxies, this is not an important effect. While we could, in principle, modify the model in an ad hoc way to reduce the surface brightnesses of dwarf galaxies, for instance by assuming a larger value of $f_{\rm diss}$ for these systems, we would then no longer fit the surface brightness versus luminosity relation for dwarfs observed in the Virgo Cluster. Of course, it is also possible that the luminosity function in the field really is similar to that in clusters, but that field dwarfs have lower surface brightnesses than cluster dwarfs because of environmental effects operating in clusters. For instance, the pressure of the intergalactic medium in clusters might make star formation more efficient, if the star formation rate is pressure regulated (Silk 1992), or it might act to confine gas that would otherwise be ejected from galaxies, as suggested by Babul & Rees (1991). However, such effects are beyond the scope of our present model.

8. The model has particular problems producing galaxies that resemble present-day bright ellipticals in their properties. Of the galaxies brighter than $\mathcal{M}_B < -18$, only 5% have the old stellar populations (age $\gtrsim 8.5$ Gyr) and red colors ($B-V > 0.8$) characteristic of present-day ellipticals. On the contrary, most galaxies with $\mathcal{M}_B < -18$ resemble rather blue spirals in their stellar populations, with half of them having $B-V < 0.5$. (The fraction of red galaxies is much larger for low-luminosity galaxies, however.) In addition, the discrepancy between predicted and observed surface brightness–luminosity relations is largest for bright ellipticals. These results suggest that some other process, not included in our model, is responsible for forming massive ellipticals. An obvious candidate for such a process is merging of mostly stellar disk galaxies. This would produce galaxies whose stellar populations are already fairly old at the time they form and which might be expected to have lower surface brightnesses than nonmerged galaxies of similar mass. The important point is that the less massive the merging objects, the older and redder will be the stellar population in the resulting product. The fraction of massive galaxies formed this way need only be 10%–20% to account for the observed fraction of bright ellipticals. There is some observational evidence for this level of merging activity from the distribution of galaxy pairs (Charlton & Salpeter 1991), and structural and line-strength peculiarities of ellipticals also provide evidence for their having undergone mergers (e.g., Schweizer et al. 1991).

It is useful to briefly compare with the results found in Paper I. There, we attempted detailed modeling only for the more massive galaxies, which were assumed not to lose any mass, and found very similar results for the luminosity function and colors of bright galaxies, although the different spectral evolution model used here results in galaxies being somewhat brighter and bluer. The contribution of mass-losing dwarf galaxies to the faint number counts was only treated schematically. We proposed that the counts at $25 \lesssim B \lesssim 27$ be explained by galaxies with $M_b \sim 10^9$–10^{10} $M_\odot$ undergoing their initial bursts of star formation at $z \sim 1$. The fully self-consistent modeling of the dwarfs in the present paper produces a similar result, except that dwarfs are seen in the counts mostly after their star formation has terminated, so the predicted redshifts are somewhat lower, $z \sim 0.2$–1.

It is also interesting to compare with the results of White & Frenk (1991), who, like us, calculated luminosity functions and number counts from a model based on the CDM scenario for galaxy formation combined with a model for star formation. Although our two models have many common features, including the use of a cooling criterion and forms of star for-

mation feedback which at low masses suppress the efficiency of converting baryons into stars by a factor proportional to the square of the halo velocity dispersion, they differ in many respects. Most important, WF assume that the only process regulating star formation is the rate at which the hot gas in halos can cool, after allowing for energy injection by young stars, while in our model, cooling of the gas is a necessary condition for star formation, but the rate of conversion of the cool gas into stars is controlled by the rate of dynamical interactions with neighboring galaxies. As a result, WF generally require rather stronger feedback than we do, affecting even bright galaxies, to avoid too large a fraction of the baryons in the universe being converted into stars, while in our model, this suppression occurs because many galaxies are in groups which have not yet collapsed and so according to our assumptions do not form any stars at all. The WF model requires fairly close coupling between star formation in the luminous part of a galaxy, and the hot gas in the surrounding halo, so the amount of cold gas awaiting conversion into stars is expected to be rather small. On the other hand, our model predicts that in many galaxies (those with a low frequency of dynamical interactions), most of the baryons should be in the form of cold gas. These two alternatives can potentially be distinguished observationally, by looking for X-ray emission from the hot gas and by looking for quasar absorption lines produced by the cold gas. Unlike our model, WF include the effects of chemical enrichment of the hot gas. However, their procedure for calculating luminosities of stellar populations is much cruder than ours, and they do not attempt to compute galaxy colors. WF present results for a range of assumptions about the baryon fraction, chemical enrichment, and amplitude of the CDM spectrum. Their best-fitting model of these has $f_b = 0.2$, $\sigma_8 = 0.4$, and includes chemical enrichment (compare to our standard model, which has $f_b = 0.2$, $\sigma_8 = 0.4$, and includes chemical enrichment (compare to our standard model, which has $f_b = 0.06$ and $\sigma_8 = 0.5$). This best-fit WF model produces a faint-end slope for the present galaxy luminosity function $\alpha \approx -1.6$, similar to our standard model, while their other models produce even steeper faint-end slopes. Their fit to the bright end of the luminosity function is somewhat poorer than ours. WF's predicted Tully-Fisher relation has circular velocities a factor ~ 2 too large at a given luminosity. WF present predictions for the number counts over the range $20 < B < 28$. Even their best-fit model falls below the observed counts by a factor ~ 4 at $B = 20$, while our standard model matches the observations to within a factor of 2 over the whole range $15 < B < 27$. WF's model predicts significantly larger redshifts than ours for the galaxies seen in the faint counts, with the distribution extending up to $z \lesssim 3$ for $B = 27$, while in our model most galaxies are at $z \lesssim 1$ at the same apparent magnitude. We expect that WF's model will suffer from similar problems with luminous galaxies being too blue as does ours, since in their model too, the most massive galaxies form at low redshifts, and will be actively forming stars at the present day.

An alternative approach to trying to produce luminosity function evolution models in an $\Omega = 1$ universe which are consistent with all the data is to assume some form of evolution in the number density of galaxies after they form. This approach has been followed by Rocca-Volmerange & Guiderdoni (1990) and Guiderdoni & Rocca-Volmerange (1991), who combine standard luminosity evolution models with phenomenological evolution of the galaxy mass function, in such a way that the total mass in galaxies is conserved. Their most successful model, which has the characteristic mass in the Schechter function varying as $M_* \propto (1 + z)^{-1.5}$, and α varying to keep the total mass constant, provides good fits to all of the observational data. In this model, the faint-end slope starts out close to $\alpha = -2$ at high redshift, and falls to $\alpha \approx -1.7$ at $z = 1$ and to $\alpha \approx -1.1$ at the present day. Guiderdoni & Rocca-Volmerange seek to explain this very strong mass function evolution by means of merging of the luminous components of galaxies. However, it remains to be seen whether the very efficient merging of low-mass galaxies that is required is reasonable on dynamical grounds, and whether it is consistent with the rather weak clustering of faint galaxies observed by Efstathiou et al. (1991) and Neuschaefer, Windhorst, & Dressler (1991).

A variety of approaches to modeling the evolution of the galaxy luminosity function thus lead to the same conclusion, that to explain the faint counts and redshift distributions in an $\Omega = 1$ universe, we require the luminosity function at $z \sim 1$ to have a steep faint-end slope, $\alpha \sim -2$. What remains in dispute is how to reconcile this with the flat slope $\alpha \approx -1$ observed for the present-day field galaxy luminosity function. The low-luminosity galaxies must be made to "disappear," either by merging them into larger systems, by reducing their present surface brightnesses and/or luminosities below visibility, or by disrupting them completely. The latter seems rather hard to achieve if star formation occurs within dark halos, since these will gravitationally confine the stars, however much gas is blown out. In this paper, we have investigated the second possibility, of fading of the stellar population after star formation is terminated by gas ejection, but found that this is not sufficiently effective, if the initial radius of the stellar population is proportional to that of the dark halo, and if the stars always form with an IMF like that in the solar neighborhood. Perhaps for low-mass galaxies outside clusters, star formation occurs while the gas is still widely dispersed throughout the halo. Alternatively, the IMF might be different in the dwarf galaxies, so that only high-mass stars form, which quickly fade after star formation ceases.

In summary, we have presented a model for galaxy luminosity function evolution that makes a number of predictions of observable properties that should soon allow further tests of the model. There remain discrepancies at low redshift, however, with the form of the luminosity function for dwarf galaxies and with the color distribution of bright galaxies. The problem with the colors could probably be alleviated by including a fairly modest amount of merging to form ellipticals, but the difficulty with the luminosity function seems to require at the least some mechanism for reducing the surface brightness of field dwarfs, relative to cluster dwarfs and to current model predictions. However, we have succeeded in explaining a remarkably wide range of observational data.

We thank Len Cowie, Raja Guhathakurta, and Tom Shanks for useful discussions, and George Efstathiou for comments on an earlier draft of this paper. C. G. L. has been supported by a SERC Advanced Fellowship. This research has been partially supported at Berkeley by NSF grant AST-8819802 awarded to J. S.

REFERENCES

Arimoto, N., & Yoshii, Y. 1986, A&A, 164, 260
———. 1987, A&A, 173, 23
Babul, A., & Rees, M. J. 1992, MNRAS, 255, 346
Bardeen, J. M., Bond, J. R., Kaiser, N., & Szalay, A. S. 1986, ApJ, 304, 15 (BBKS)
Barnes, J., & Efstathiou, G. 1987, ApJ, 319, 575
Binggeli, B. 1985, in Star Forming Dwarf Galaxies and Related Objects, ed. D. Kunth, T. X. Thuam, & J. Tran Thanh Van (Gif sur Yvette: Editions Frontiéres), 53
Binggeli, B., Sandage, A., & Tarenghi, M. 1984, AJ, 89, 64
Binggeli, B., Tarengi, M., & Sandage, A. 1990, A&A, 228, 42
Blumenthal, G. R., Faber, S. M., Primack, J. R., & Rees, M. J. 1984, Nature, 311, 517
Bothun, G., Impey, D. I., & Malin, D. F. 1991, ApJ, 376, 404
Briggs, F. H. 1990, AJ, 100, 999
Broadhurst, T. J., Ellis, R. S., & Shanks, T. 1988, MNRAS, 235, 827
Brown, R. L. 1988, in QSO Absorption Lines, ed. J. C. Blades, D. Turnshek, & C. A. Norman (Cambridge Univ. Press) 291
Bruzual, G. 1981, Ph.D. thesis, University of California, Berkeley
———. 1983, ApJ, 273, 105 (B83)
Bruzual, G., & Kron, R. G. 1980, ApJ, 241, 25
Carlberg, R. G. 1991, ApJ, 367, 385
Charlot, S., & Bruzual, G. 1991, ApJ, 367, 126
Charlton, J. C., & Salpeter, E. E. 1991, ApJ, 375, 517
Cole, S., Treyer, M., & Silk, J. 1992, ApJ, 385, 9
Colless, M., Ellis, R. S., Taylor, K., Hook, R. N. 1990, MNRAS, 244, 408
Cowie, L. L., Songaila, A., & Hu, E. M. 1991, Nature, 354, 460
Davis, M., Efstathiou, G., Frenk, C. S., & White, S. D. M. 1985, ApJ, 292, 371
Dekel, A. 1991, in Physical Cosmology, ed. A. Blanchard, L. Celnikier, M. Lachieze-Rey, & J. Tran Thanh Van (Gif-sur-Yvette: Editions Frontiéres), 309
Dekel, A., & Silk, J. 1986, ApJ, 303, 39
de Vaucouleurs, G. 1977, in The Evolution of Galaxies and Stellar Populations, ed. B. M. Tinsley & R. B. Larson (New Haven: Yale Univ. Obs.), 43
Djorgovski, S., & Davis, M. 1987, ApJ, 313, 59
Dressler, A. 1980, ApJ, 236, 351
Dressler, A., Lynden-Bell, D., Burstein, D., Davies, R. L., Faber, S. M., Terlevich, R. J., & Wegner, G. 1987, ApJ, 313, 42
Efstathiou, G., Bernstein, G., Katz, N., Tyson, J. A., & Guhathakurta, P. 1991, ApJ, 380, L47
Efstathiou, G., Frenk, C. S., White, S. D. M., & Davis, M. 1988, MNRAS, 235, 715
Efstathiou, G. P. 1992, MNRAS, in press
Faber, S. M., Wegner, G., Burstein, D., Davies, R. L., Dressler, A., Lynden-Bell, D., & Terlevich, R. J. 1989, ApJS, 69, 763
Fall, S. M. 1983, in IAU Symp. 100, Internal Kinematics and Dynamics of Galaxies, ed. E. Athanassoula (Dordrecht: Reidel), 391
———. 1987, in Nearly Normal Galaxies, ed. S. M. Faber (New York: Springer), 326
Fall, S. M., & Rees, M. J. 1985, ApJ, 298, 18
Ferguson, H. C., & Sandage, A. 1991, ApJ, 101, 765
Fisher, J. R., & Tully, R. B. 1981, ApJ, 243, L23
Frenk, C. S., White, S. D. M., Davis, M., & Efstathiou, G. 1988, ApJ, 327, 507
Glazebrook, K. 1991, Ph.D. thesis, University of Edinburgh
Guiderdoni, B. 1991, in The Early Observable Universe from Diffuse Backgrounds, ed. B. Rocca-Volmerange, J. M. Deharveng, & J. Tran Thanh Van (Gif-sur-Yvette: Editions Frontiéres), 193
Guiderdoni, B., & Rocca-Volmerange, B. 1987, A&A, 186, 1 (GRV87)
———. 1989, in The Epoch of Galaxy Formation, ed. C. S. Frenk, R. S. Ellis, A. Heavens, J. Peacock, & T. Shanks (Dordrecht: Kluwer), 367
———. 1990a, A&A, 227, 362
———. 1990b, in Particle Astrophysics: The Early Universe and Cosmic Structures, ed. J. M. Alimi, A. Blanchard, A. Bouquet, F. Martin de Volnay, & J. Tran Thanh Van (Gif-sur-Yvette: Editions Frontiéres), 355
———. 1991, A&A, 252, 435
Gunn, J. E. 1982, in Astrophysical Cosmology, ed. H. A. Bruck, G. V. Coyne, & M. S. Longair (Vatican City: Pontificià Academià Scientiarum), 233
Heydon-Dumbleton, N., Collins, C. A., & McGillivray, H. 1989, MNRAS, 238, 379
Impey, C., Bothun, G., & Malin, D. 1988, ApJ, 330, 634
Infante, L., Pritchett, C., & Quintana, H. 1986, ApJ, 91, 217
Jarvis, J. F., & Tyson, J. A. 1981, AJ, 83, 1549
Jones, L. R., Fong, R., Shanks, T., Ellis, R. S., & Peterson, B. A. 1991, MNRAS, 249, 481
Kawano, L., Schramm, D., & Steigman, G. 1988, ApJ, 330, L1
Kennicutt, R. C. 1983, ApJ, 272, 54
Kennicutt, R. C. Keel, W. C., van der Hulst, J. M., Hummel, E., & Roettiger, K. A. 1987, AJ, 1011
Koo, D. C. 1985, AJ, 90, 418
———. 1986, ApJ, 311, 651
———. 1990, in Evolution of the Universe of Galaxies: The Edwin Hubble Centennial Symp., ed. R. G. Kron (San Francisco: ASP), 268
Kraan-Korteweg, R. C., Cameron, L. M., & Tamman, G. A. 1988, ApJ, 331, 620
Kron, R. G. 1980, ApJS, 43, 305
Lacey, C. G. 1991, in The Early Observable Universe from Diffuse Backgrounds, ed. B. Rocca-Volmerange, J. M. Deharveng, & J. Tran Thanh Van (Gif-sur-Yvette: Editions Frontiéres), 315
Lacey, C. G., & Silk, J. 1991, ApJ, 381, 14 (Paper I)
Larson., R. B. 1974, MNRAS, 169, 229
Larson, R. B., & Tinsley, B. M. 1978, ApJ, 219, 46
Lilly, S. J., Cowie, L. L., & Gardner, J. P. 1991, ApJ, 369, 79
Lonsdale, C. J., Persson, S. E., & Matthews, K. 1984, ApJ, 287, 95
Loveday, J., Peterson, B. A., Efstathiou, G., & Maddox, S. J. 1992, MNRAS, ApJ, 390, 338
Maddox, S. J., Efstathiou, G., Sutherland, W. J., & Loveday, J. 1990a, MNRAS, 242, 43P
Maddox, S. M., Sutherland, W. J., Efstathiou, G., Loveday, J., & Peterson, B. A. 1990b, MNRAS, 247, 1P
Maeder, A., & Meynet, G. 1988, A&AS, 76, 411
Metcalfe, N., Shanks, T., Fong, R., & Jones, L. R. 1991, MNRAS, 249, 498
Milgrom, M. 1988, A&A, 202, L9
Mochkovitch, R., & Rocca-Volmerange, B. 1984, A&A, 137, 298
Neuschaefer, L. W., Windhorst, R. A., & Dressler, A. 1991, ApJ, 382, 32
Nieto, J. L., Bender, R., Davoust, E., & Prugniel, P. 1990, A&A, 230, L17
Noguchi, M. 1990, in The Interstellar Medium in Galaxies, ed. H. A. Thronson & J. M. Shull (Dordrecht: Kluwer), 323
Peterson, B. A., Ellis, R. S., Kibblewhite, E. J., Bridgeland, M. T., Hooley, T., & Horne, D. 1979, ApJ, 233, L109
Postman, M., & Geller, M. J. 1984, ApJ, 281, 95
Rocca-Volmerange, B. 1989, MNRAS, 236, 47
———. 1992, in IAU Symp. 149, The Stellar Populations of Galaxies, ed. B. Barbuy (Dordrecht: Reidel), 357
Rocca-Volmerange, B., & Guiderdoni, B. 1988, A&AS, 75, 93
———. 1990, MNRAS, 247, 166
Rocca-Volmerange, B., Lequeux, J., & Maucherat-Joubert, M. 1981, A&A, 104, 177
Rubin, V. C., Burstein, D., Ford, W. K., & Thonnard, N. 1985, ApJ, 289, 81
Sandage, A. 1983, in IAU Symp. 100, Internal Kinematics and Dynamics of Galaxies, ed. E. Athanassoula (Dordrecht: Reidel), 367
Sandage, A., Binggeli, B., & Tamman, G. A. 1985, AJ, 90, 1759
Scalo, J. M. 1986, Fund. Cosmic Phys., 11, 1
Schweizer, F., et al. 1990, ApJ, 364, L33
Silk, J. 1992, ApJ, submitted
Tinsley, B. M. 1980, ApJ, 241, 41
Toomre, A. 1981, in The Structure and Evolution of Normal Galaxies, ed. S. M. Fall & D. Lynden-Bell (Cambridge Univ. Press), 111
Turnshek, D. A., Wolfe, A. M., Lanzetta, K. M., Briggs, F. H., Cohen, R. D., Foltz, C. B., Smith, H. E., & Wilkes, B. J. 1989, ApJ, 344, 567
Tyson, J. A. 1988, AJ, 96, 1
VandenBerg, D. A. 1985, ApJS, 58, 711
Walker, T. P., Steigman, G., Schramm, D. N., Olive, K. A., & Kang, H.-S. 1991, ApJ, 376, 51
Weinberg, S. 1972, Gravitation and Cosmology (New York: Wiley)
White, S. D. M., & Frenk, C. S. 1991, ApJ, 379, 52 (WF)
White, S. D. M., & Rees, M. J. 1978, MNRAS, 183, 341
Yoshii, Y., & Peterson, B. A. 1991, ApJ, 372, 8
Yoshii, Y., & Takahara, F. 1988, ApJ, 326, 1
Zurek, W. H., Quinn, P. J., & Salmon, J. K. 1988, ApJ, 330, 519